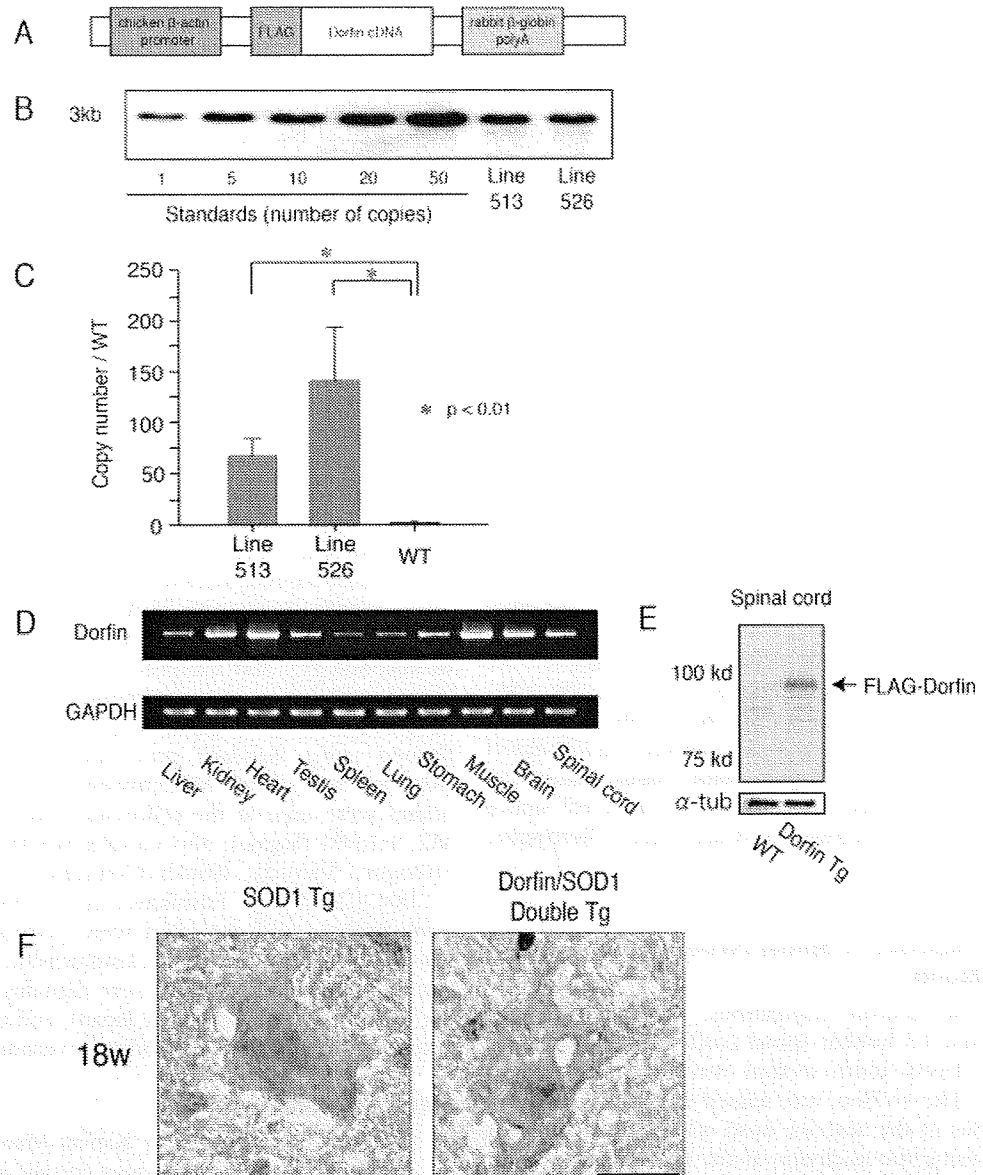

Fig. 1. Dorfin transgenic mouse. **A:** Schematic view of the transgene constructs. The microinjected fragment was composed of a chicken β-actin promoter, a FLAG-tagged Dorfin, and a rabbit β-globin polyadenylation signal sequence (poly-A). **B:** Southern blot analysis of Dorfin transgenic mouse tail DNA. About 20 copies of FLAG-Dorfin transgene are detected in DNA samples from lines 513 and 526. **C:** Quantitative RT-PCR analysis of Dorfin mRNA expression. Total RNA samples were extracted from spinal cord of Dorfin Tg and wt mice (*$P < 0.01$; n = 3 each). Dorfin Tg mice from both lines 513 and 526 express Dorfin mRNA at significantly higher levels than wt mice. Error bars represent SEM. **D:** Transgene expression in Dorfin 526 line Tg mice. RT-PCR analysis of RNA from systemic organs. **E:** Dorfin protein in the spinal cord of 526 Dorfin Tg mouse. Immunoprecipitation using anti-FLAG antibody demonstrates that exogenous FLAG-Dorfin is detected only in Dorfin Tg mice. **F:** Immunohistochemistry of the spinal cord of 526 Dorfin/G93A SOD1 double Tg mice and G93A SOD1 Tg mice with antibodies against Dorfin. Scale bar = 20 μm.

essed for paraffin embedding, as previously described (Adachi et al., 2001; Katsuno et al., 2002). Transverse sections of spinal cord (4 μm thick) were deparaffinized, rehydrated, and treated for antigen retrieval. For the mutant SOD1 immunohistochemical study, the paraffin sections were pretreated with formic acid for 5 min at room temperature; processed using the Ventana Discovery system (Ventana, Tucson, AZ) with heating at 100°C for 30 min; and incubated with mouse anti-SOD1Ab, NCL-SOD1 (1:5,000; Novocastra, Newcastle upon Tyne, United Kingdom), and biotin-SP-conjugated goat anti-mouse IgG (1:500; Jackson Immunoresearch, West Grove, PA) using the Ventana DAB map kit (Ventana, Tucson, AZ). For immunostaining of ubiquitin, sections were similarly processed and incubated with antiubiquitin mouse monoclonal antibody 4PD1 (1:1,000; Santa Cruz Biotechnology, Santa Cruz, CA) and biotin-SP-conjugated goat anti-mouse IgG

(1:500; Jackson Immunoresearch). The areas of SOD1-positive immunoreactivity or ubiquitin-positive aggregates in the anterior horn of transverse spinal cord sections were assessed with a computer-assisted image analyzer (Win roof; Mitani Corporation, Tokyo, Japan) under the light microscope (Axio Imager M1; Carl Zeiss Japan, Tokyo, Japan). Each spinal cord section was divided into four portions by coronal and sagittal lines passing through the central canal. The immunoreactive areas in the gray matter of the above-mentioned dorsal portions were summed and divided by the area of the entire gray matter of the same portion to calculate the ratio of the immunoreactive area. One hundred consecutive transverse sections of the lumbar spinal cord were prepared for each of five mice, and SOD1- or ubiquitin-positive areas in the anterior horn were assessed on every tenth section, as described previously (Terao et al., 1996). For Dorfin immunohistochemistry, we air dried cryostat sections (6 μm thick) of mice spinal cord (Katsuno et al., 2003) and stained them with antiserum against Dorfin (Dorfin-41, 1:200; Niwa et al., 2001; Hishikawa et al., 2003). For double-immunofluorescence staining of the spinal cord, sections were blocked with 4% goat serum and then sequentially incubated with anti-GFAP antibody (1:1,000; Dako, Glostrup, Denmark) and anti-SOD1 antibody (1:100; NCL-SOD1). Anti-GFAP antibody was visualized by anti-rabbit goat IgG coupled with Alexa Fluor 488 (Molecular Probes, Eugene, OR), and anti-SOD1 antibody was visualized with anti-mouse goat IgG coupled with Alexa Fluor 568 (Molecular Probes). Stained sections were observed under an LSM-710 confocal microscope (Carl Zeiss, Gottingen, Germany).

Morphometric Analyses of Spinal Neurons and Ventral Spinal Roots

To assess the neuron populations, 100 serial (4 μm thick) sections from L5 lumbar spinal cords were prepared as described above. Every tenth section was examined by the disector method. The section was stained by the Nissl technique, and neurons in the anterior horn were counted by the disector method using the nucleolus as the leading edge on an Axio vision image analyzer (Carl Zeiss Japan) as described previously (Terao et al., 1996; West, 1999). Data were expressed as the number of neurons per volume of 400 μm thickness of unilateral ventral horn.

The L5 ventral roots were fixed in 2.5% glutaraldehyde in 0.125 M cacodylate buffer (pH 7.4) and embedded in epoxy resin for morphometric analysis. Morphological changes and diameters of myelinated fibers with normal shape were assessed in toluidine blue-stained semithin sections. Morphological changes of myelinated fibers were assessed as described previously (Dyck et al., 1993). Abnormal fibers were those with swollen axons or with a myelin ovoid showing the figure of axonal change (Dyck et al., 1993). Normally shaped myelinated fibers were chosen manually, and their diameters were measured using a computer-assisted image analyzer (Axiovision; Carl Zeiss Japan, Tokyo, Japan), as described previously (Katsuno et al., 2002; Minamiyama et al., 2004). The results were expressed as a diameter frequency histogram per whole L5 ventral root using the data from normally shaped fibers. The ratio of the normally shaped small fibers (<6 μm) and normally shaped large fibers (≥6 μm) to the number of normally shaped fibers at 10 weeks, 14 weeks, and 18 weeks of age were investigated. The ratio of the number of abnormal fibers against the normal and abnormal fibers was examined.

Immunoprecipitation and Western Blotting Analysis

Spinal cords were snap-frozen with powdered CO_2 in acetone (Katsuno et al., 2003). Frozen tissue was homogenized in ice-cold lysis buffer (50 mM HEPES, pH 7.4, 150 mM NaCl, 10 mM EDTA, 1% NP-40), maintained at 4°C for 30 min, and centrifuged at 18,000*g* for 30 min at 4°C. The protein concentration of the supernatant (soluble fraction) was determined by using the DC protein assay (Bio-Rad). The pellet fractions were suspended in ice-cold buffer (0.5% SDS, 8 M urea, 1% β-mercaptoethanol, 50 mM phosphate buffer, pH 7. 4), homogenized 15 times, and kept at 4°C for 30 min. Samples were then centrifuged at 18,000*g* for 30 min at 4°C to obtain the supernatant (insoluble fraction).

Immunoprecipitation from the soluble fraction was performed with 8 μg anti-FLAG rabbit antibody (Sigma, St. Louis, MO) and Protein A/G Plus-Agarose (Santa Cruz Biotechnology), and the precipitates were washed four times. Spinal cord lysates or immunoprecipitates were separated by SDS-PAGE (5–20% gradient gel). Western blotting was performed using standard procedures as described previously (Katsuno et al., 2002; Minamiyama et al., 2004). Primary antibodies were used at the following concentrations: anti-FLAG M2, 1:1,000 (Sigma); anti-Cu-Zn SOD1, 1:5,000 (SOD-100; Stressgen, Victoria, British Columbia, Canada); anti-Dorfin, 1:1,000 (Dorfin 30; Hishikawa et al., 2003). Secondary antibody probing and detection were performed using the ECL Plus kit (GE Healthcare, Buckinghamshire, United Kingdom). Chemiluminescence signals were digitalized (LAS-3000 Imaging System; Fujifilm, Tokyo, Japan), and band intensities were quantified in Multi Gauge software version 3.0 (Fujifilm).

Statistical Analyses

Data were analyzed by Kaplan-Meier and log-rank tests for survival rate, unpaired *t*-tests for the results of RT-PCR, two-factor repeated measure ANOVA for the Rotarod and footprint, one-factor factorial ANOVA with Fisher's probability of least significant differences post hoc test for the results of immunohistochemical study with SOD1 and ubiquitin antibody, and two-factor factorial ANOVA for the other analyses (Statview version 5; Hulinks, Tokyo, Japan). *P* values of 0.05 or less denoted statistical significance.

RESULTS

Dorfin Transgenic Mice

We established 20 lines of Dorfin transgenic mice and examined 10 different organs for exogenous, FLAG-tagged Dorfin mRNA expression. We assessed the number of copies of Dorfin transgene in each Dorfin Tg mouse line by Southern blotting (Fig. 1B) and quantitative RT-PCR (Fig. 1C) and selected two Dorfin Tg mouse lines for further study (513 and 526). Approximately 20 copies of the FLAG-Dorfin transgene were

TABLE I. Copy Number of Mutant SOD1 Gene*

Genotype	G93A mutant SOD1 copy number
Dorfin/G93A mSOD1 double Tg	25.2 ± 1.6
G93A mSOD1 Tg	25.0 ± 1.1

*Values are the mean ± SD, n = 72 (Dorfin/G93A mSOD1 double Tg), n = 77 (G93A mSOD1 Tg).

detected in DNA samples from each of these lines. Exogenous Dorfin was highly expressed in the spinal cord, brain, muscles, kidney, heart, and testis and was not substantially detected in the stomach, lung, spleen, or liver (Fig. 1D). We were unable to detect the exogenous Dorfin protein by Western blotting, probably because of its short half-life (Ishigaki et al., 2007). Immunoprecipitation using anti-FLAG antibody showed that exogenous Dorfin protein was detected only in the Dorfin Tg mice (Fig. 1E). We also detected Dorfin protein by immunohistochemistry with Dorfin antibody in Dorfin/G93A SOD1 double Tg mouse spinal cord sections (Fig.1F). We did not find differences in size, body weight, gross morphology, or behavior between the Dorfin Tg mice and their littermates, indicating that Dorfin overexpression does not affect normal mouse development.

Dorfin Ameliorates Clinical Phenotypes in a Transgenic Mouse Model of ALS

To determine the potential neuroprotective role of Dorfin in mutant SOD1-related ALS, progeny of Dorfin transgenic mice (lines 513 and 526) were crossed with G93A mutant SOD1 transgenic mice [B6SJL-TgN (SOD1-G93A)1Gur] (Gurney et al., 1994). The mean copy number of the mutant SOD1 gene in mice used for examinations is shown in Table I. The same copy number was observed in Dorfin/G93A SOD1 double Tg mice and G93A SOD1 Tg mice. We determined the life span and assessed motor impairment in both lines of Dorfin/G93A SOD1 double Tg mice and G93A SOD1 Tg mice. Dorfin/G93A SOD1 double Tg mice survived significantly longer than SOD1 Tg offspring from crossings of either Dorfin Tg line (Fig. 2A). Dorfin improved the mean survival time (513 Dorfin/G93ASOD1 double Tg at 144.9 days vs. G93ASOD1 Tg at 134.4 days, $P < 0.01$; and 526 Dorfin/G93ASOD1 double Tg at 142.2 days vs. G93ASOD1 Tg at 131.7 days, $P < 0.01$) as well as the maximal life span (513 Dorfin/G93ASOD1 Double Tg at 175 days vs. G93A SOD1 Tg at 155 days and 526 Dorfin/G93ASOD1 Double Tg at 167 days vs. G93A SOD1 Tg at 148 days; Fig. 2A). Both Dorfin Tg lines showed a significant increase in the mean life span of approximately 10 days and a significant increase in maximal life span of approximately 20 days. As a measure of motor impairment, we assessed Rotarod performance and foot stride during walking. The onset of motor impairment on the Rotarod task was delayed for 1 week in both lines of Dorfin/G93A SOD1 double Tg mice, and the progression of the motor deficit was slowed by 1–2 weeks compared with that observed in the G93A SOD1 Tg mice. Both the 513 and the 526 lines of Dorfin/G93A SOD1 double Tg mice performed significantly better than the G93A SOD1 Tg mice ($P < 0.05$, ANOVA; Fig. 2B; 513: Dorfin/G93ASOD1 double Tg 300 ± 0.0 sec vs. G93ASOD1 Tg 300 ± 0.0 sec at 10 weeks of age, 300 ± 0.0 sec vs. 278.8 sec at 14 weeks of age, 160.8 ± 34.2 sec vs. 67.8 ± 25.5 sec at 18 weeks of age; 526: 300 ± 0.0 sec vs. 300 ± 0.0 sec at 10 weeks of age, 300 ± 0.0 sec vs. 300 ± 0.0 sec at 14 weeks of age, 135.8 ± 29.8 sec vs. 86.0 ± 27.0 sec at 18 weeks of age). We analyzed the walking strides at three time points, 10 weeks (presymptomatic stage), 14 weeks (early stage), and 18 weeks of age (end stage). Both lines of Dorfin/G93ASOD1 double Tg mice showed significantly longer foot strides than the G93A SOD1 Tg mice (513: $P < 0.05$; 526: $P < 0.01$, ANOVA; Fig. 2C; 513: Dorfin/G93ASOD1 double Tg 68.0 ± 2.0 mm vs. G93ASOD1 Tg 63.0 ± 0.9 mm at 10 weeks of age, 69.7 ± 2.3 mm vs. 63.6 ± 0.9 mm at 14 weeks of age, 29.9 ± 5.8 mm vs. 20.1 ± 3.0 mm at 18 weeks of age; 526: 67.3 ± 1.8 mm vs. 67.1 ± 0.9 mm at 10 weeks of age, 63.1 ± 1.3 mm vs. 63.3 ± 1.4 mm at 14 weeks of age, 50.1 ± 5.6 mm vs. 26.0 ± 4.5 mm at 18 weeks of age).

Dorfin Ameliorates Histopathological Changes in the Transgenic Mouse Model of ALS

Dorfin ameliorated histopathological impairments in spinal neurons (Fig. 3A) and their axons in the double Tg mice (Fig. 3B). We assessed the size of the neuron population in the lumbar spinal cord and the distribution of ventral root diameters. The number of neurons in the unilateral lumbar spinal anterior horn was significantly larger in the Dorfin 526/G93ASOD1 double Tg mice than in the G93ASOD1 Tg mice examined with ANOVA ($P < 0.05$; n = 5). Dorfin overexpression also ameliorated histopathological changes in the ventral roots. Histograms of the diameters of myelinated fibers in the G93ASOD1 Tg mouse lumbar ventral roots showed decreases in the numbers of large myelinated fibers with age, whereas the 526 Dorfin/G93ASOD1 double Tg mice retained these large axons even at 18 weeks of age (Fig. 3B). We investigated the ratio of normally shaped small myelinated fibers (<6 μm) and normally shaped large myelinated fibers (≥6 μm) to the normally shaped fibers (Fig. 3C), and the ratio of abnormally shaped fibers to the normally shaped and abnormally shaped fibers (Fig. 3D) at 10 weeks, 14 weeks, and 18 weeks of age with ANOVA. Dorfin/G93ASOD1 double Tg mice showed a significantly lower ratio of small myelinated fibers ($P < 0.05$, ANOVA) and a higher ratio of large myelinated fibers ($P < 0.05$, ANOVA) compared with G93A SOD1 Tg mice. The ratio of abnormal fibers in Dorfin/G93ASOD1 double Tg mice was significantly lower than that of G93ASOD1 Tg mice ($P < 0.05$, ANOVA).

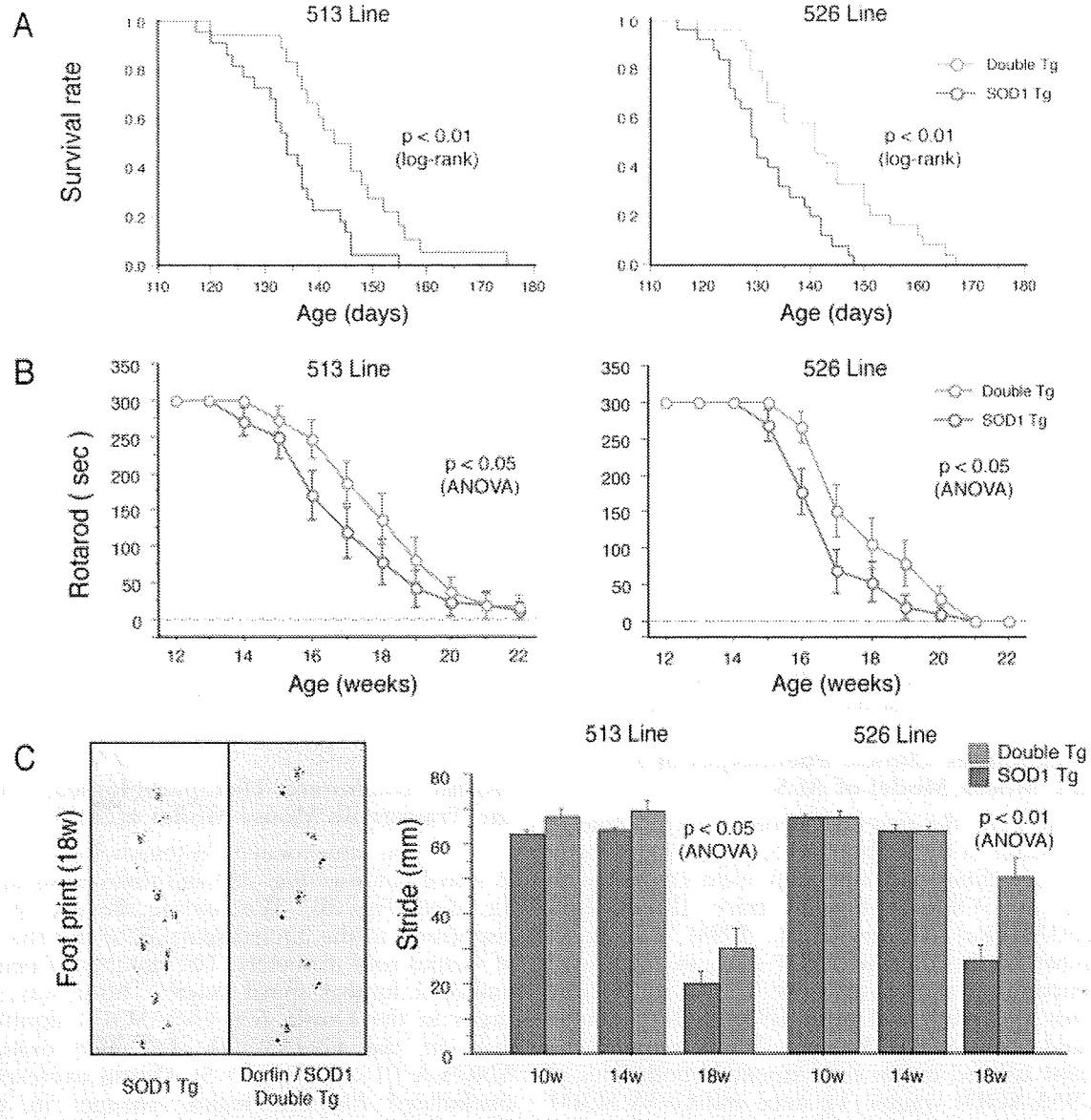

Fig. 2. Dorfin ameliorates clinical phenotypes of G93A mutant SOD1 Tg mice. **A:** Survival rate (Kaplan-Meier). Dorfin/G93A SOD1 double Tg mice of both lines 513 and 526 (green) show significantly longer survival times than the G93A SOD1 Tg mice ($P < 0.01$ log-rank). **B:** Rotarod task. Both 513 and 526 lines of Dorfin/G93A SOD1 double Tg mice perform significantly better on the Rotarod task than the G93A SOD1 Tg mice ($P < 0.05$, ANOVA). **C:** Left: Footprints of 526 line mice at 18 weeks of age. Front paws are in red and hind paws in blue. Right: Dorfin/G93A SOD1 double Tg mice of both lines show longer strides than the G93A SOD1 Tg mice (513: $P < 0.05$, 526: $P < 0.01$, ANOVA). The number of mice was 513 line: n = 18 (male = 10, female = 8) in Dorfin/G93ASOD1 double Tg and n = 22 (male = 8, female = 14) in G93A SOD1 Tg; 526 line: n = 24 (male = 12, female = 12) in Dorfin/G93ASOD1 double Tg and n = 25 (male = 9, female = 16) in G93A SOD1 Tg. Values represents means ± SEM.

Dorfin Decreases the Amount of Mutant SOD1 in the Spinal Cord of SOD1 Tg Mice

As we reported previously (Niwa et al., 2002), the overexpression of Dorfin accelerated the degradation of mutant SOD1 protein by the ubiquitin-proteasome system. We investigated the ability of Dorfin to reduce the amount of mutant SOD1 protein using immunohistochemistry at 18 weeks of age and Western blotting of mice spinal cords from line 526 mice (Figs. 4, 5). In transverse sections of the ventral horn (Fig. 4A), the SOD1-positive areas from Dorfin/G93ASOD1 double Tg mice were significantly smaller than those in G93ASOD1 Tg mice (Fig. 4B; Dorfin/G93ASOD1 double Tg at 2.66% vs. G93ASOD1 Tg at 3.45%, $P < 0.01$). Immunohistochemistry with antiubiquitin antibody revealed that ubiquitin-positive protein accumulations were present in the cytoplasm of the residual motor neurons and also in the neuropil (Fig. 4C). The

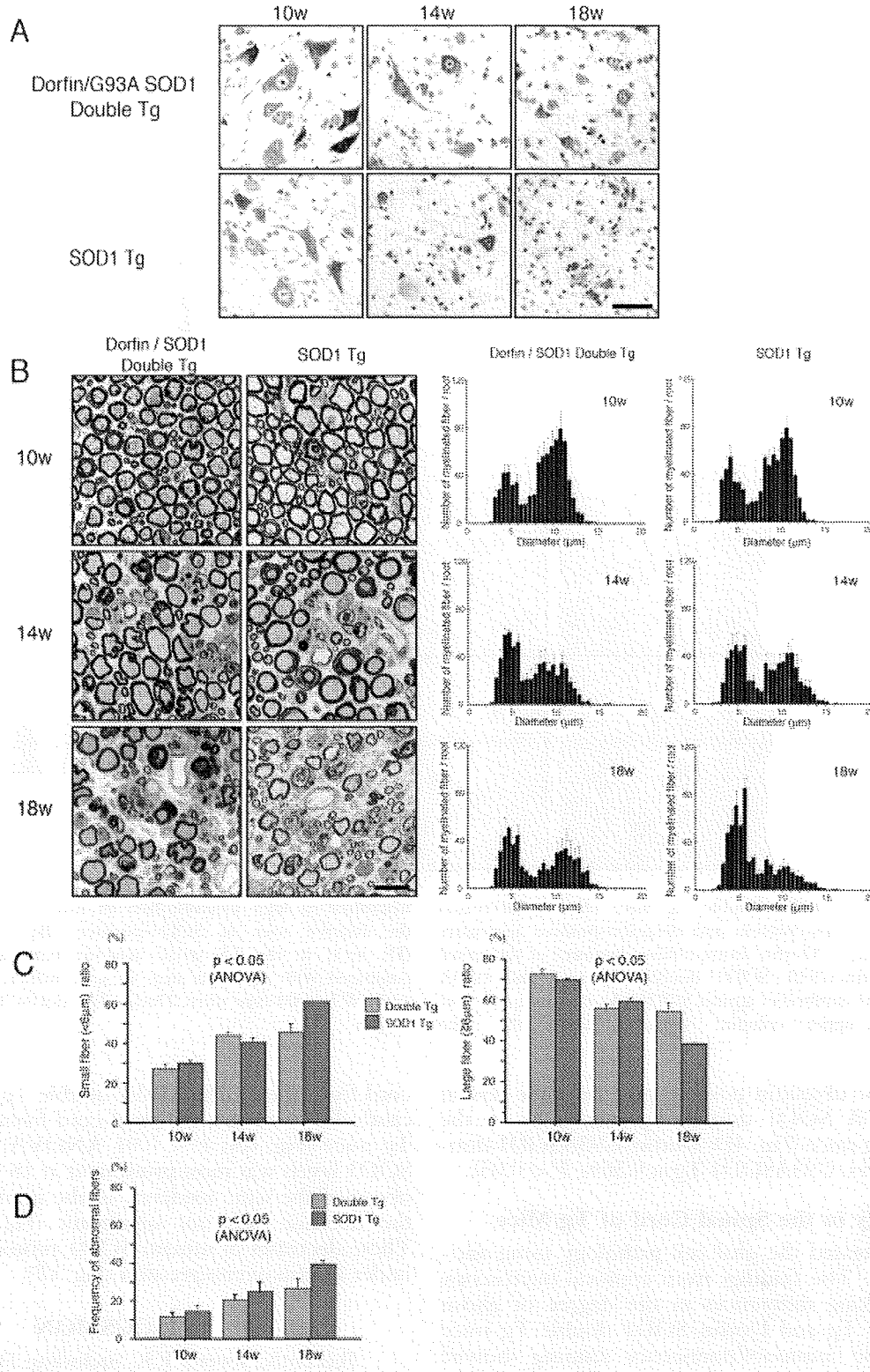

Fig. 3. Histopathological analysis of spinal cord and ventral roots of 526 Dorfin/G93A mutant SOD1 double Tg mice and G93A mutant SOD1 Tg mice. **A:** Transverse section of Nissl-stained L5 spinal anterior horns of 526 Dorfin/G93A mutant SOD1 double Tg mice and G93A mutant SOD1 Tg mice at 10 weeks, 14 weeks, and 18 weeks of age. **B:** Transverse, semithin section of L5 ventral roots stained with toluidine blue at 10 weeks, 14 weeks, and 18 weeks of age. Histograms of the diameters of myelinated fibers in the ventral roots show that the progressive decrease in the number of large myelinated fibers was suppressed in Dorfin/G93A SOD1 double Tg mice compared with G93A SOD1 Tg mice at 18 weeks (n = 3). **C:** Bar graphs of the small fiber ratio (%) of the ventral root ($P < 0.05$, ANOVA) and bar graphs of the large fiber ratio (%) of the ventral root ($P < 0.05$, ANOVA). **D:** The frequency of abnormal fibers. Dorfin/G93A SOD1 double Tg mice show a significantly lower frequency of abnormal fibers than G93A SOD1 Tg mice ($P < 0.05$, ANOVA). Scale bars = 50 μm in A; 20 μm in B. [Color figure can be viewed in the online issue, which is available at www.interscience.wiley.com.]

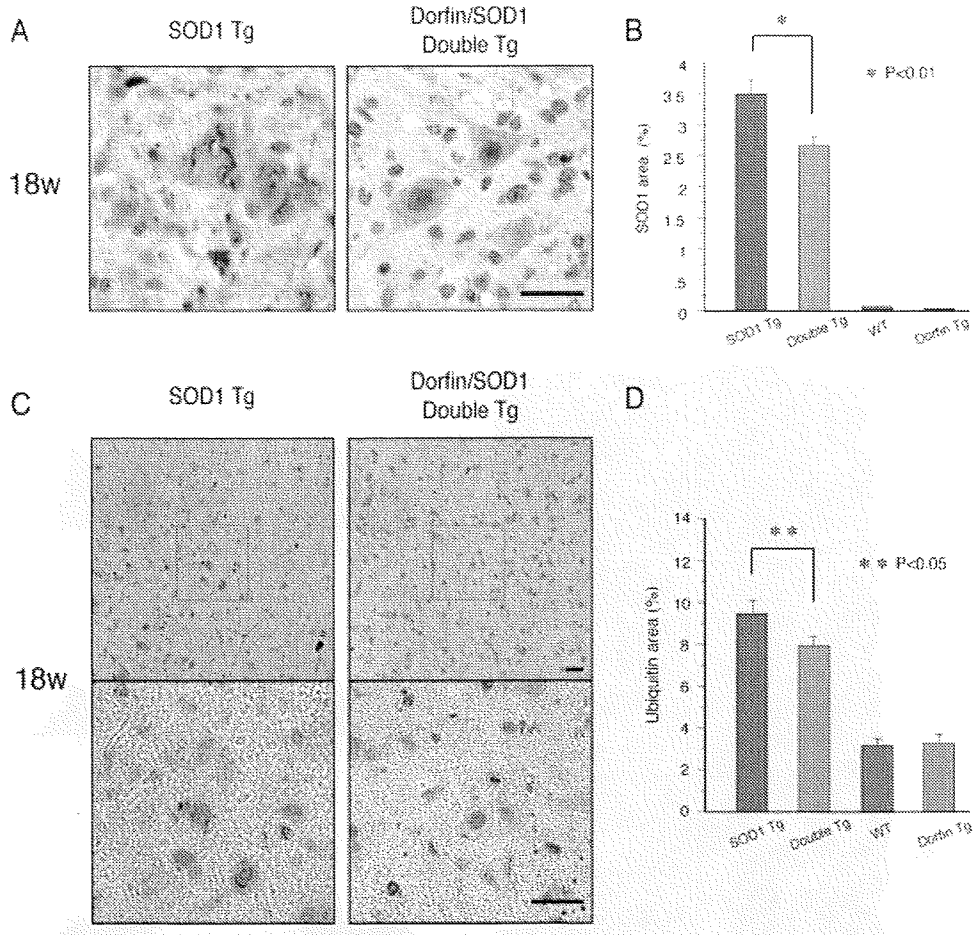

Fig. 4. Dorfin/G93A SOD1 double Tg mice show a decreased amount of mutant SOD1 protein and ubiquitin-positive aggregates under overexpression of Dorfin. Immunohistochemistry of the spinal cord of 526 Dorfin/G93A SOD1 double Tg mice and G93A SOD1 Tg mice with antibodies against SOD1 (**A**), ubiquitin (**C**; low magnification in upper column; square indicates the area magnified in high magnification in lower column). Bar graphs of the relative sizes of SOD1-positive (**B**) and ubiquitin-positive (**D**) areas in the L5 spinal anterior horn at 18 weeks of age compared with the total areas of gray matter. $*P < 0.01$, $**P < 0.05$. WT, wild-type mice, Dorfin Tg;, dorfin Tg mice. Scale bars = 20 μm.

accumulations of ubiquitin-positive proteins were less in the Dorfin/G93A SOD1 double Tg mice than in the G93A SOD1 Tg mice (Fig. 4D; Dorfin/G93ASOD1 double Tg at 7.99% vs. G93ASOD1 Tg at 9.56%, $P < 0.05$).

Glial Pathology in the Spinal Cord of Tg Mice

We investigated the glial cell pathology using anti-GFAP antibody. The findings from confocal microscopy showed no striking differences in the degree of gliosis between SOD1 Tg and Dorfin/SOD1 double Tg mice (Fig. 5). Double immunofluorescence staining showed that SOD1-positive inclusion was not observed in the cytoplasm of astrocytes in the spinal cords of both SOD1 Tg and Dorfin/SOD1 double Tg mice.

Western Blot Analysis in the Spinal Cord of Tg Mice

Results from Western blotting analysis showed that the level of mutant SOD1 in the soluble fraction of spinal cord from the Dorfin/G93A double Tg mice was significantly less than that of spinal cord from the G93ASOD1 Tg mice (Fig. 6A; $P < 0.01$ ANOVA). The decrease in SOD1 levels was most prominent at 18 weeks of age. We observed the same tendency in the insoluble fraction, but the decrease was not significant (Fig. 6B; ANOVA). These decreases of mutant SOD1 proteins were observed under Dorfin overexpression (Fig. 1F).

DISCUSSION

Recently, several E3s, including Dorfin, were identified that specifically recognize and reduce the levels of mutant SOD1 protein in an in vitro cell culture model (Niwa et al., 2002; Miyazaki et al., 2004; Urushitani et al., 2004). However, these results have not been verified in vivo. In the present study, we demonstrated for the first time that transgenically overexpressed Dorfin, as an E3, attenuates the accumulation of mutant SOD1 deposition, reduces neuronal death and axonal degenera-

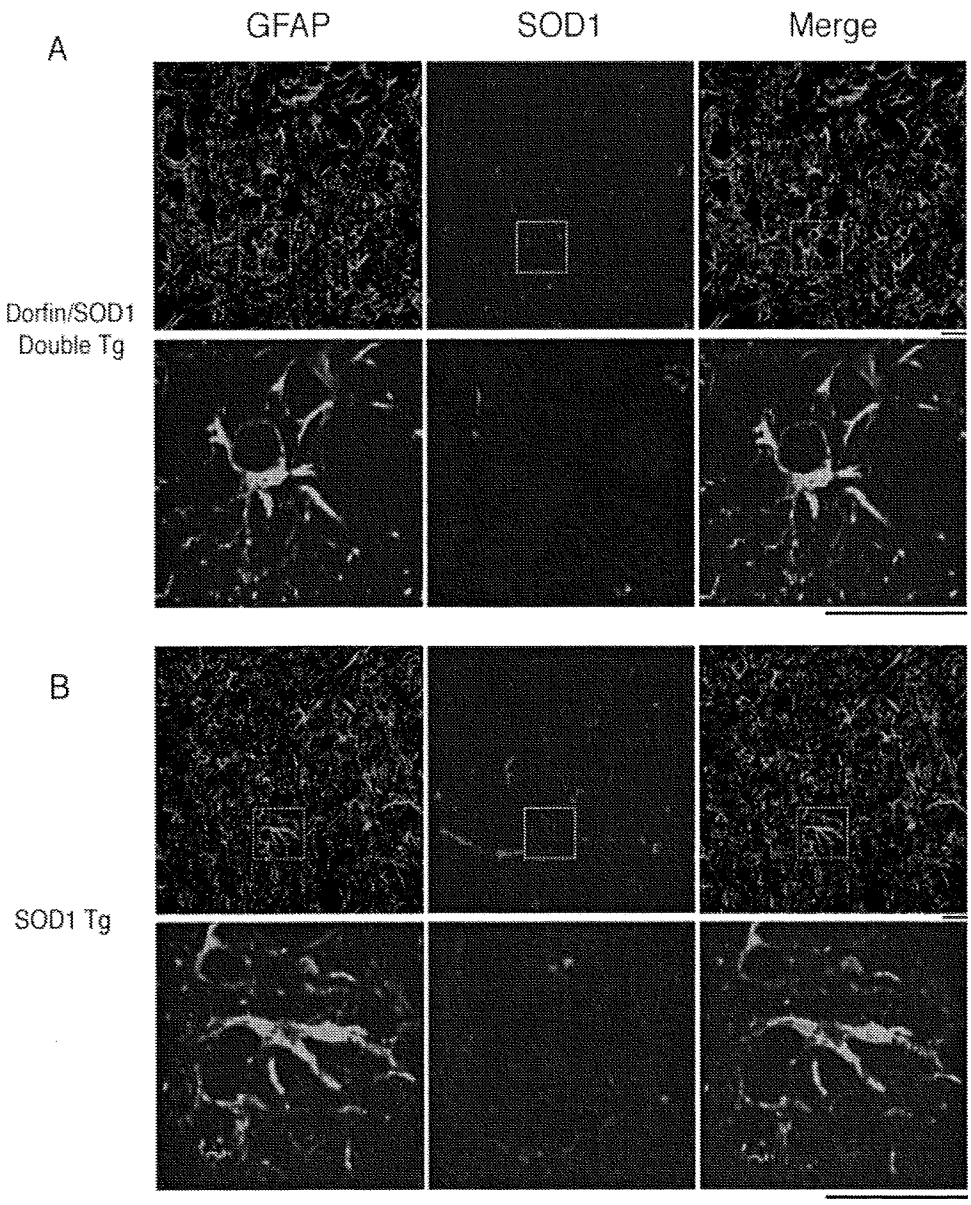

Fig. 5. Imunofluorescence study of the spinal cord of 526 Dorfin/G93A SOD1 double Tg mice (**A**) and G93A SOD1 Tg mice (**B**) using antibodies against GFAP and SOD1. Low magnification at upper column and high magnification in lower column (The square indicates the area magnified in high magnification in lower column). The findings revealed no striking differences in the degree of gliosis between SOD1 Tg and Dorfin/SOD1 double Tg. SOD1 protein was not localized in astrocytes. Scale bars = 20 μm.

tion of motor neurons, ameliorates motor performance deficits, and extends the life span of G93A SOD1 transgenic mice.

The E3 CHIP was reported to degrade toxic misfolded proteins associated with molecular chaperons Hsp70 and Hsp90 (McDonough and Patterson, 2003; Shin et al., 2005; Dickey et al., 2006) and to ameliorate the phenotypes of transgenic mouse (Adachi et al., 2007) and zebrafish (Miller et al., 2005) models of polyglutamine disease. These reports suggest that the overexpression of this E3 is beneficial for rescuing the phenotype of neurodegenerative disease.

As opposed to CHIP, Dorfin specifically recognizes mutant SOD1 molecules and degrades them via the ubiquitin-proteasome system (Niwa et al., 2001, 2002). This specific recognition suggests an advantage for using Dorfin as a therapeutic tool against mutant SOD1-mediated ALS.

SALS, FALS, and G93A mutant SOD1 Tg mice have been reported to present ubiquitin-positive aggregation (Murayama et al., 1990; Watanabe et al., 2001; Ardley and Robinson, 2004). In this study, we demonstrated a reduction in mutant SOD1 protein and ubiquitin-positive protein accumulation in the spinal cord

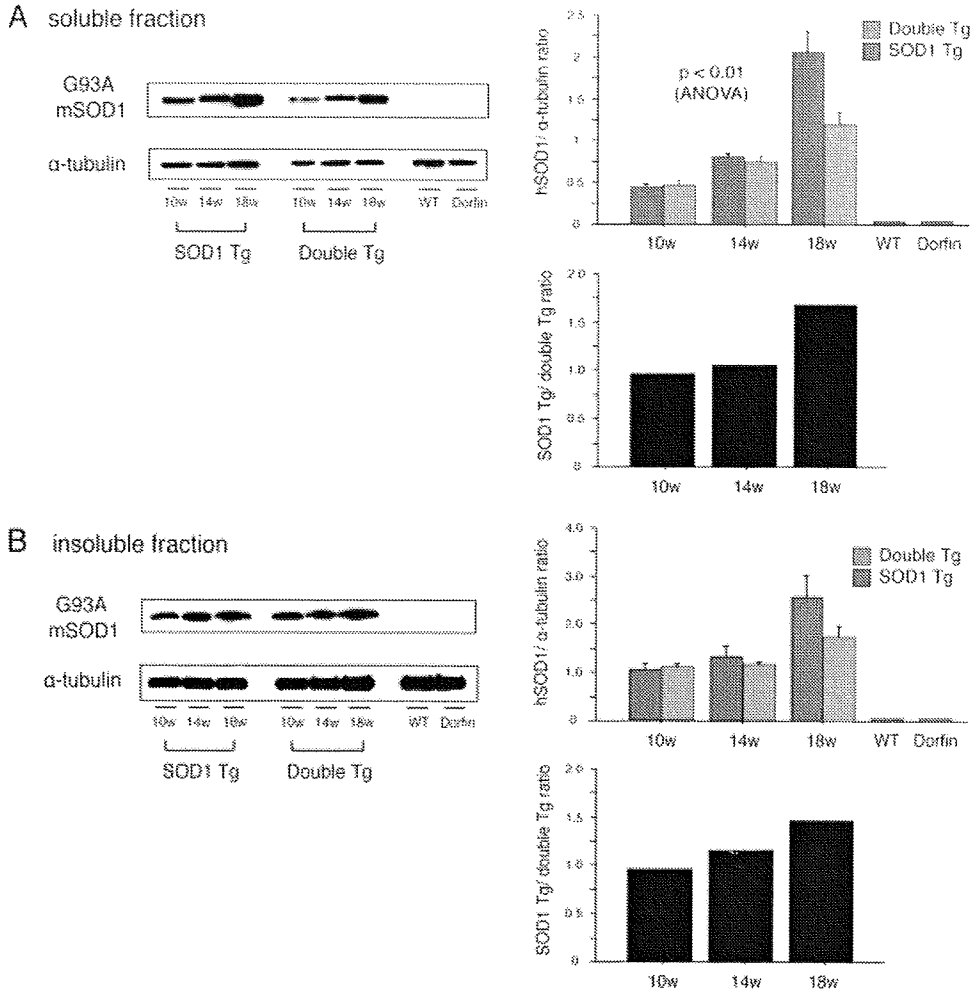

Fig. 6. Western blot analysis of the spinal cord protein extracts from 526 Dorfin/G93A SOD1 double Tg mice and G93A SOD1 Tg mice. Western blotting was performed at 10, 14, and 18 weeks of age using anti-Cu-Zn SOD1 antibody. Soluble fraction (**A**), insoluble fraction (**B**). Each lane contains 10 μg protein. Bar graphs in each case represent the densitometric analysis of the standardized amount of SOD1 protein against endogenous α-tubulin in each Western blot and the ratio of SOD1 Tg/Dorfin/SOD1 double Tg standardized data of at each age. Protein samples were prepared from each of five different mice and averaged in the quantification. Error bars represent SEM. WT, wild-type littermate; Dorfin, dorfin Tg. [Color figure can be viewed in the online issue, which is available at www.interscience.wiley.com.]

resulting from Dorfin overexpression. On Western blots, the reduction of mutant SOD1 was more marked in the soluble fraction from end-stage mice than in the insoluble fraction. Thus, Dorfin overexpression may reduce more soluble mutant SOD1 protein. Dorfin also reduced the histopathological deposition of mutant SOD1 and ubiquitin-positive protein in the spinal cord at 18 weeks of age. Overaccumulation of ubiquitinated, misfolded proteins may adversely affect the proteasome machinery and impair normal protein degradation (Boillee et al., 2006). Thus, a reduction of this deposition may lead to reduced cytotoxicity of spinal neurons and, finally, to the amelioration of histopathological and clinical phenotypes.

These results were consistent with those of our previous study showing that Dorfin overexpression protected against the toxic effects of mutant SOD1 in neuronal cell culture (Niwa et al., 2002). Dorfin overexpression reduced the levels of mutant SOD1 by recognizing and ubiquitinating mutant SOD1 proteins and by targeting them for proteasomal degradation, thereby protecting against neuronal cell death (Niwa et al., 2002, 2007).

Histopathological amelioration as assessed by observing the number of neurons in the anterior horn and ventral root was detected. The number of abnormal fibers was decreased, and the population of large fibers was well preserved in Dorfin/G93A SOD1 double Tg mice compared with G93A SOD1 Tg mice. From these results, we infer that Dorfin overexpression has a protective effect against axonal degeneration caused by G93A mutant SOD1 protein. These histopathological ameliorations may lead to the improvement of clinical phenotypes as indicated by improvements in the Rotarod tasks and foot strides reported here, although there was no

remarkable difference in the degree of gliosis in the spinal cords. Many reports have suggested that not only motor neurons but also other cell types, such as astrocytes, play an important role in neurodegeneration (Pramatarova et al., 2001; Clement et al., 2003; Boillee et al., 2006). In our examination, we observed that SOD1 positive aggregates existed in the cell body of neurons, but there were no aggregates observed in astrocytes from either G93A SOD1 Tg or Dorfin/SOD1 double Tg mice. This result suggests that the overexpressed Dorfin was unable to ubiquitinate G93A mutant SOD1 protein in the astrocytes because there was no accumulation of G93A mutant SOD1 protein in the astrocytes of G93A SOD1 Tg mice. Consequently, Dorfin may have no beneficial effect on the astrocyte cell function impaired by mutant SOD1 protein.

Although many hypotheses for the pathogenesis of ALS have been proposed (Julien, 2001; Boillee et al., 2006; Kabashi and Durham, 2006; Van Deerlin et al., 2008), we suggest that a reduction in the levels of mutant SOD1 may have a beneficial effect on neuronal cell viability, including mitochondria function and a potential for therapeutic use (Niwa et al., 2002; Takeuchi et al., 2004).

In the present study, Dorfin overexpression was effective in ameliorating the ALS phenotypes of the G93A SOD1 Tg mouse but was not as efficient as treatment with VEGF or IGF-1 delivered via the lentivirus system (Kaspar et al., 2003; Azzouz et al., 2004). One reason for this reduced efficacy may be that transgenically expressed Dorfin does not clear sufficient amounts of mutant SOD1 protein to eliminate the phenotypes because of its short half-life (Ishigaki et al., 2007). Dorfin may be precisely regulated in its expression level in vivo, and, thus, exogenously expressed human Dorfin under the β-actin promoter may be degraded immediately. Moreover, as the pathology of the G93A SOD1 mouse progresses, the function of the proteasome gradually deteriorates (Kabashi et al., 2004; Cheroni et al., 2005; Boillee et al., 2006; Cheroni et al., 2009), and Dorfin may lose its E3 activity to clear the mutant SOD1 with advancing disease. Strategies to improve the activity of Dorfin include the utilization of a Dorfin-CHIP chimeric protein, which has the E3 activity of Dorfin and a longer half-life, as we reported previously (Ishigaki et al., 2007), and, alternatively, the crossing of the Dorfin Tg mouse with other mutant SOD1 Tg mouse showing milder symptoms with a slower progressive course than G93A. In these cases, Dorfin may exert a more marked amelioration of the phenotypes. In the present study, the gender balance of the mice was different to some extent between Dorfin/SOD1 double Tg and SOD1 Tg in both the 513 and the 526 lines (percentage of male mice 513: 55% for Dorfin/SOD1 double Tg, 36.3% for SOD1 Tg; 526: 50% for Dorfin/SOD1 double Tg, 36% for SOD1 Tg). The differences in SOD1 Tg motor function and survival between males and females has been reported previously (Mahoney et al., 2004; Stam et al., 2008). Female mice showed a longer survival and better motor function, and the difference of gender balance may contribute to a modest difference of survival or motor function.

The important point of this study is that the overexpression of a toxic protein-specific E3 that reacts specifically and directly with mutant SOD1 ameliorated the clinical and pathological phenotypes of mutant SOD1-mediated motor neuron degeneration. Dorfin has been shown in previous studies to localize to various inclusions found in neurological tissue samples of human disease. For SALS, the Lewy body-like inclusions were immunoreactive for anti-Dorfin antibody, and, for FALS, the hyaline-like inclusions were positive for Dorfin (Hishikawa et al., 2003; Ito et al., 2003). These findings suggest that Dorfin may be involved in the pathogenesis of a broad spectrum of neurodegenerative disorders (Hishikawa et al., 2003; Ito et al., 2003) and may provide a clue to the treatment of these diseases. The activation or induction of the E3 Dorfin may be an effective therapeutic strategy for a wide range of neurodegenerative diseases.

REFERENCES

Adachi H, Kume A, Li M, Nakagomi Y, Niwa H, Do J, Sang C, Kobayashi Y, Doyu M, Sobue G. 2001. Transgenic mice with an expanded CAG repeat controlled by the human AR promoter show polyglutamine nuclear inclusions and neuronal dysfunction without neuronal cell death. Hum Mol Genet 10:1039–1048.

Adachi H, Waza M, Tokui K, Katsuno M, Minamiyama M, Tanaka F, Doyu M, Sobue G. 2007. CHIP overexpression reduces mutant androgen receptor protein and ameliorates phenotypes of the spinal and bulbar muscular atrophy transgenic mouse model. J Neurosci 27:5115–5126.

Alves-Rodrigues A, Gregori L, Figueiredo-Pereira ME. 1998. Ubiquitin, cellular inclusions and their role in neurodegeneration. Trends Neurosci 21:516–520.

Ardley HC, Robinson PA. 2004. The role of ubiquitin-protein ligases in neurodegenerative disease. Neurodegen Dis 1:71–87.

Azzouz M, Ralph GS, Storkebaum E, Walmsley LE, Mitrophanous KA, Kingsman SM, Carmeliet P, Mazarakis ND. 2004. VEGF delivery with retrogradely transported lentivector prolongs survival in a mouse ALS model. Nature 429:413–417.

Boillee S, Vande Velde C, Cleveland DW. 2006. ALS: a disease of motor neurons and their nonneuronal neighbors. Neuron 52:39–59.

Bruijn LI, Houseweart MK, Kato S, Anderson KL, Anderson SD, Ohama E, Reaume AG, Scott RW, Cleveland DW. 1998. Aggregation and motor neuron toxicity of an ALS-linked SOD1 mutant independent from wild-type SOD1. Science 281:1851–1854.

Cassina P, Cassina A, Pehar M, Castellanos R, Gandelman M, de Leon A, Robinson KM, Mason RP, Beckman JS, Barbeito L, Radi R. 2008. Mitochondrial dysfunction in SOD1G93A-bearing astrocytes promotes motor neuron degeneration: prevention by mitochondrial-targeted antioxidants. J Neurosci 28:4115–4122.

Cheroni C, Peviani M, Cascio P, Debiasi S, Monti C, Bendotti C. 2005. Accumulation of human SOD1 and ubiquitinated deposits in the spinal cord of SOD1G93A mice during motor neuron disease progression correlates with a decrease of proteasome. Neurobiol Dis 18:509–522.

Cheroni C, Marino M, Tortarolo M, Veglianese P, De Biasi S, Fontana E, Zuccarello LV, Maynard CJ, Dantuma NP, Bendotti C. 2009. Functional alterations of the ubiquitin-proteasome system in motor neurons of a mouse model of familial amyotrophic lateral sclerosis. Hum Mol Genet 18:82–96.

Ciechanover A. 2005. Intracellular protein degradation: from a vague idea thru the lysosome and the ubiquitin-proteasome system and onto human diseases and drug targeting. Cell Death Differ 12:1178–1190.

Clement AM, Nguyen MD, Roberts EA, Garcia ML, Boillee S, Rule M, McMahon AP, Doucette W, Siwek D, Ferrante RJ, Brown RH Jr, Julien JP, Goldstein LS, Cleveland DW. 2003. Wild-type nonneuronal cells extend survival of SOD1 mutant motor neurons in ALS mice. Science 302:113–117.

Dal Canto MC, Mourelatos Z, Gonatas NK, Chiu A, Gurney ME. 1996. Neuropathological changes depend on transgene copy numbers in transgenic mice for mutant human Cu, Zn superoxide dismutase (SOD). In: Nakano I, Hirano A, editors. Amyotrophic lateral sclerosis: progress and perspectives in basic research and clinical application. Amsterdam: Elsevier Science. p 331–338.

Dickey CA, Yue M, Lin WL, Dickson DW, Dunmore JH, Lee WC, Zehr C, West G, Cao S, Clark AM, Caldwell GA, Caldwell KA, Eckman C, Patterson C, Hutton M, Petrucelli L. 2006. Deletion of the ubiquitin ligase CHIP leads to the accumulation, but not the aggregation, of both endogenous phospho- and caspase-3-cleaved tau species. J Neurosci 26:6985–6996.

Dyck PJ, Giannini C, Lais A. 1993. Pathologic alterations of nerves. In: Dyck PJ, Thomas PK, Griffin JW, Low PA, Poduslo JF, editors. Peripheral neuropathy, 3rd ed. Philadelphia: W.B. Saunders. p 514–595.

Goldberg AL. 2003. Protein degradation and protection against misfolded or damaged proteins. Nature 426:895–899.

Gurney ME, Pu H, Chiu AY, Dal Canto MC, Polchow CY, Alexander DD, Caliendo J, Hentati A, Kwon YW, Deng HX, et al. 1994. Motor neuron degeneration in mice that express a human Cu,Zn superoxide dismutase mutation. Science 264:1772–1775.

Hirano A. 1996. Neuropathology of ALS: an overview. Neurology 47(Suppl 2):S63–S66.

Hishikawa N, Niwa J, Doyu M, Ito T, Ishigaki S, Hashizume Y, Sobue G. 2003. Dorfin localizes to the ubiquitylated inclusions in Parkinson's disease, dementia with Lewy bodies, multiple system atrophy, and amyotrophic lateral sclerosis. Am J Pathol 163:609–619.

Ishigaki S, Liang Y, Yamamoto M, Niwa J, Ando Y, Yoshihara T, Takeuchi H, Doyu M, Sobue G. 2002. X-Linked inhibitor of apoptosis protein is involved in mutant SOD1-mediated neuronal degeneration. J Neurochem 82:576–584.

Ishigaki S, Niwa J, Yamada S, Takahashi M, Ito T, Sone J, Doyu M, Urano F, Sobue G. 2007. Dorfin-CHIP chimeric proteins potently ubiquitylate and degrade familial ALS-related mutant SOD1 proteins and reduce their cellular toxicity. Neurobiol Dis 25:331–341.

Ito T, Niwa J, Hishikawa N, Ishigaki S, Doyu M, Sobue G. 2003. Dorfin localizes to Lewy bodies and ubiquitylates synphilin-1. J Biol Chem 278:29106–29114.

Julien JP. 2001. Amyotrophic lateral sclerosis. unfolding the toxicity of the misfolded. Cell 104:581–591.

Kabashi E, Durham HD. 2006. Failure of protein quality control in amyotrophic lateral sclerosis. Biochim Biophys Acta 1762:1038–1050.

Kabashi E, Agar JN, Taylor DM, Minotti S, Durham HD. 2004. Focal dysfunction of the proteasome: a pathogenic factor in a mouse model of amyotrophic lateral sclerosis. J Neurochem 89:1325–1335.

Kabuta T, Suzuki Y, Wada K. 2006. Degradation of amyotrophic lateral sclerosis-linked mutant Cu,Zn-superoxide dismutase proteins by macroautophagy and the proteasome. J Biol Chem 281:30524–30533.

Kaspar BK, Llado J, Sherkat N, Rothstein JD, Gage FH. 2003. Retrograde viral delivery of IGF-1 prolongs survival in a mouse ALS model. Science 301:839–842.

Katsuno M, Adachi H, Kume A, Li M, Nakagomi Y, Niwa H, Sang C, Kobayashi Y, Doyu M, Sobue G. 2002. Testosterone reduction prevents phenotypic expression in a transgenic mouse model of spinal and bulbar muscular atrophy. Neuron 35:843–854.

Katsuno M, Adachi H, Doyu M, Minamiyama M, Sang C, Kobayashi Y, Inukai A, Sobue G. 2003. Leuprorelin rescues polyglutamine-dependent phenotypes in a transgenic mouse model of spinal and bulbar muscular atrophy. Nat Med 9:768–773.

Mahoney DJ, Rodriguez C, Devries M, Yasuda N, Tarnopolsky MA. 2004. Effects of high-intensity endurance exercise training in the G93A mouse model of amyotrophic lateral sclerosis. Muscle Nerve 29:656–662.

Martin LJ, Liu Z, Chen K, Price AC, Pan Y, Swaby JA, Golden WC. 2007. Motor neuron degeneration in amyotrophic lateral sclerosis mutant superoxide dismutase-1 transgenic mice: mechanisms of mitochondriopathy and cell death. J Comp Neurol 500:20–46.

McDonough H, Patterson C. 2003. CHIP: a link between the chaperone and proteasome systems. Cell Stress Chaperones 8:303–308.

Miller VM, Nelson RF, Gouvion CM, Williams A, Rodriguez-Lebron E, Harper SQ, Davidson BL, Rebagliati MR, Paulson HL. 2005. CHIP suppresses polyglutamine aggregation and toxicity in vitro and in vivo. J Neurosci 25:9152–9161.

Minamiyama M, Katsuno M, Adachi H, Waza M, Sang C, Kobayashi Y, Tanaka F, Doyu M, Inukai A, Sobue G. 2004. Sodium butyrate ameliorates phenotypic expression in a transgenic mouse model of spinal and bulbar muscular atrophy. Hum Mol Genet 13:1183–1192.

Miyazaki K, Fujita T, Ozaki T, Kato C, Kurose Y, Sakamoto M, Kato S, Goto T, Itoyama Y, Aoki M, Nakagawara A. 2004. NEDL1, a novel ubiquitin-protein isopeptide ligase for dishevelled-1, targets mutant superoxide dismutase-1. J Biol Chem 279:11327–11335.

Murayama S, Mori H, Ihara Y, Bouldin TW, Suzuki K, Tomonaga M. 1990. Immunocytochemical and ultrastructural studies of lower motor neurons in amyotrophic lateral sclerosis. Ann Neurol 27:137–148.

Niwa J, Ishigaki S, Doyu M, Suzuki T, Tanaka K, Sobue G. 2001. A novel centrosomal ring-finger protein, dorfin, mediates ubiquitin ligase activity. Biochem Biophys Res Commun 281:706–713.

Niwa J, Ishigaki S, Hishikawa N, Yamamoto M, Doyu M, Murata S, Tanaka K, Taniguchi N, Sobue G. 2002. Dorfin ubiquitylates mutant SOD1 and prevents mutant SOD1-mediated neurotoxicity. J Biol Chem 277:36793–36798.

Niwa J, Yamada S, Ishigaki S, Sone J, Takahashi M, Katsuno M, Tanaka F, Doyu M, Sobue G. 2007. Disulfide bond mediates aggregation, toxicity, and ubiquitylation of familial amyotrophic lateral sclerosis-linked mutant SOD1. J Biol Chem 282:28087–28095.

Pramatarova A, Laganiere J, Roussel J, Brisebois K, Rouleau GA. 2001. Neuron-specific expression of mutant superoxide dismutase 1 in transgenic mice does not lead to motor impairment. J Neurosci 21:3369–3374.

Rosen DR, Siddique T, Patterson D, Figlewicz DA, Sapp P, Hentati A, Donaldson D, Goto J, O'Regan JP, Deng HX, et al. 1993. Mutations in Cu/Zn superoxide dismutase gene are associated with familial amyotrophic lateral sclerosis. Nature 362:59–62.

Ross CA, Poirier MA. 2004. Protein aggregation and neurodegenerative disease. Nat Med 10(Suppl):S10–S17.

Rowland LP, Shneider NA. 2001. Amyotrophic lateral sclerosis. N Engl J Med 344:1688–1700.

Sherman MY, Goldberg AL. 2001. Cellular defenses against unfolded proteins: a cell biologist thinks about neurodegenerative diseases. Neuron 29:15–32.

Shibata N, Asayama K, Hirano A, Kobayashi M. 1996. Immunohistochemical study on superoxide dismutases in spinal cords from autopsied patients with amyotrophic lateral sclerosis. Dev Neurosci 18:492–498.

Shin Y, Klucken J, Patterson C, Hyman BT, McLean PJ. 2005. The co-chaperone carboxyl terminus of Hsp70-interacting protein (CHIP) mediates alpha-synuclein degradation decisions between proteasomal and lysosomal pathways. J Biol Chem 280:23727–23734.

Stam NC, Nithianantharajah J, Howard ML, Atkin JD, Cheema SS, Hannan AJ. 2008. Sex-specific behavioural effects of environmental

enrichment in a transgenic mouse model of amyotrophic lateral sclerosis. Eur J Neurosci 28:717–723.

Strong MJ, Kesavapany S, Pant HC. 2005. The pathobiology of amyotrophic lateral sclerosis: a proteinopathy? J Neuropathol Exp Neurol 64:649–664.

Takeuchi H, Niwa J, Hishikawa N, Ishigaki S, Tanaka F, Doyu M, Sobue G. 2004. Dorfin prevents cell death by reducing mitochondrial localizing mutant superoxide dismutase 1 in a neuronal cell model of familial amyotrophic lateral sclerosis. J Neurochem 89:64–72.

Terao S, Sobue G, Hashizume Y, Li M, Inagaki T, Mitsuma T. 1996. Age-related changes in human spinal ventral horn cells with special reference to the loss of small neurons in the intermediate zone: a quantitative analysis. Acta Neuropathol 92:109–114.

Urushitani M, Kurisu J, Tsukita K, Takahashi R. 2002. Proteasomal inhibition by misfolded mutant superoxide dismutase 1 induces selective motor neuron death in familial amyotrophic lateral sclerosis. J Neurochem 83:1030–1042.

Urushitani M, Kurisu J, Tateno M, Hatakeyama S, Nakayama K, Kato S, Takahashi R. 2004. CHIP promotes proteasomal degradation of familial ALS-linked mutant SOD1 by ubiquitinating Hsp/Hsc70. J Neurochem 90:231–244.

Van Deerlin VM, Leverenz JB, Bekris LM, Bird TD, Yuan W, Elman LB, Clay D, Wood EM, Chen-Plotkin AS, Martinez-Lage M, Steinbart E, McCluskey L, Grossman M, Neumann M, Wu IL, Yang WS, Kalb R, Galasko DR, Montine TJ, Trojanowski JQ, Lee VM, Schellenberg GD, Yu CE. 2008. TARDBP mutations in amyotrophic lateral sclerosis with TDP-43 neuropathology: a genetic and histopathological analysis. Lancet Neurol 7:409–416.

Watanabe M, Dykes-Hoberg M, Culotta VC, Price DL, Wong PC, Rothstein JD. 2001. Histological evidence of protein aggregation in mutant SOD1 transgenic mice and in amyotrophic lateral sclerosis neural tissues. Neurobiol Dis 8:933–941.

West MJ. 1999. Stereological methods for estimating the total number of neurons and synapses: issues of precision and bias. Trends Neurosci 22:51–61.

THE JOURNAL OF BIOLOGICAL CHEMISTRY VOL. 284, NO. 33, pp. 22059–22066, August 14, 2009

TDP-43 Depletion Induces Neuronal Cell Damage through Dysregulation of Rho Family GTPases*

Received for publication, March 5, 2009, and in revised form, June 9, 2009 Published, JBC Papers in Press, June 17, 2009, DOI 10.1074/jbc.M109.012195

Yohei Iguchi[‡], Masahisa Katsuno[‡§], Jun-ichi Niwa[¶], Shin-ichi Yamada[‡], Jun Sone[‡], Masahiro Waza[‡], Hiroaki Adachi[‡], Fumiaki Tanaka[‡], Koh-ichi Nagata[‖], Nariko Arimura[**], Takashi Watanabe[§‡‡], Kozo Kaibuchi[‡‡], and Gen Sobue[‡1]

From the Departments of [‡]Neurology and [‡‡]Cell Pharmacology, Nagoya University Graduate School of Medicine, Showa-ku, Nagoya 466-8550, [§]Institute for Advanced Research, Nagoya University, Nagoya 464-8601, [¶]Stroke Center, Aichi Medical University, Aichi 480-1195, [‖]Department of Molecular Neurobiology, Institute for Developmental Research, Aichi Human Service Center, Aichi 480-0838, and [**]Tamagawa University Brain Science Institute, Tokyo 194-8610, Japan

The 43-kDa TAR DNA-binding protein (TDP-43) is known to be a major component of the ubiquitinated inclusions characteristic of amyotrophic lateral sclerosis and frontotemporal lobar degeneration with ubiquitin-positive inclusions. Although TDP-43 is a nuclear protein, it disappears from the nucleus of affected neurons and glial cells, implicating TDP-43 loss of function in the pathogenesis of neurodegeneration. Here we show that the knockdown of TDP-43 in differentiated Neuro-2a cells inhibited neurite outgrowth and induced cell death. In knockdown cells, the Rho family members RhoA, Rac1, and Cdc42 GTPases were inactivated, and membrane localization of these molecules was reduced. In addition, TDP-43 depletion significantly suppressed protein geranylgeranylation, a key regulating factor of Rho family activity and intracellular localization. In contrast, overexpression of TDP-43 mitigated the cellular damage caused by pharmacological inhibition of geranylgeranylation. Furthermore administration of geranylgeranyl pyrophosphate partially restored cell viability and neurite outgrowth in TDP-43 knockdown cells. In summary, our data suggest that TDP-43 plays a key role in the maintenance of neuronal cell morphology and survival possibly through protein geranylgeranylation of Rho family GTPases.

The 43-kDa TAR DNA-binding protein (TDP-43)[2] has recently been identified as a major component of the ubiquitinated inclusions characteristic of amyotrophic lateral sclerosis (ALS) and frontotemporal lobar degeneration with ubiquitin-positive inclusions (1, 2). Subsequently several point mutations located in the glycine-rich domain of TDP-43 have been identified as the disease-causing mutations of familial and sporadic ALS (3–7). TDP-43 has been shown to be a fundamental component of ubiquitin-positive neuronal cytoplasmic and intranuclear inclusions as well as that of neuronal dystrophic neurites in the affected neurons or glial cells in these neurodegenerative diseases. TDP-43 is known to regulate gene transcription, exon splicing, and exon inclusion through interactions with RNA, heterogeneous nuclear ribonucleoproteins, and nuclear bodies (8–12). Recently it has been reported that TDP-43 stabilizes human low molecular weight neurofilament mRNA through direct interaction with the 3′-untranslated region (13) and that it regulates retinoblastoma protein phosphorylation through the repression of cyclin-dependent kinase 6 expression (14). However, the physiological function of TDP-43 in the central nervous system has not been fully elucidated, and it remains unclear how this protein is implicated in the pathogenesis of neurodegeneration.

The Rho family of GTPases are members of the Ras superfamily and are known for regulating actin cytoskeletal dynamics (15–18). RhoA, Rac1, and Cdc42, the most studied proteins of this family, also modulate functions such as cell movement, motility, transcription, cell growth, and cell survival (18). In neurons, RhoA, Rac1, and Cdc42 have been shown to regulate neurite outgrowth (19–21).

Although TDP-43 is localized in the nucleus of unaffected neurons, nuclear staining of this protein is significantly reduced in neurons bearing ubiquitin inclusions (1, 2, 22), suggesting that loss of TDP-43 function may play a role in neurodegeneration. In this study, we used small interfering RNA (siRNA) to investigate the effect of TDP-43 loss of function on cell death and neurite outgrowth and elucidated a novel relation between TDP-43 and the activities of RhoA, Rac1, and Cdc42.

EXPERIMENTAL PROCEDURES

siRNA Oligonucleotides and Construction of Expression Vectors—The oligonucleotide siRNA duplex was synthesized by Takara Bio (Shiga, Japan). The siRNA sequences were as follows: scrambled (control) siRNA-set1, 5′-GAAUCAGAUGCACAUGAGUTT-3′; -set2, 5′-ACGGCCUAAUCUAACAGACTT-3′; TDP-43 siRNA-set1, 5′-GAACGAUGAACCCAUUGAATT-3′; -set2, 5′-CCAAUGCUGAACCUAAGCATT-3′. Unless otherwise mentioned, set 1 siRNA was used for TDP-43 knockdown throughout the experiments.

* This work was supported by a Center-of-Excellence grant from the Ministry of Education, Culture, Sports, Science and Technology of Japan; grants from the Ministry of Health, Labor and Welfare of Japan; a grant from the Japan Intractable Diseases Research Foundation; and the Program for Improvement of Research Environment for Young Researchers from Special Coordination Funds for Promoting Science and Technology commissioned by the Ministry of Education, Culture, Sports, Science and Technology.

[1] To whom correspondence should be addressed: Dept. of Neurology, Nagoya University Graduate School of Medicine, 65 Tsurumai-cho, Showa-ku, Nagoya 466-8550, Japan. Fax: 81-52-7442785; E-mail: sobueg@med.nagoya-u.ac.jp.

[2] The abbreviations used are: TDP-43, 43-kDa TAR DNA-binding protein; ALS, amyotrophic lateral sclerosis, siRNA, small interfering RNA; MTS, 3-(4,5-dimethylthiazol-2-yl)-5-(3-caboxymethoxyphenyl)-2-(4-sulfophenyl)-2*H*-tetrazolium; GGPP, geranylgeranyl pyrophosphate; MVA, mevalonic acid; PI, propidium iodide; TUNEL, terminal deoxynucleotidyltransferase dUTP nick end labeling; GAPDH, glyceraldehyde-3-phosphate dehydrogenase.

The pEGFP-Rac1 construct was produced as described elsewhere (23, 24). Mouse TDP-43 (GenBank™ accession number NM_145556) cDNA was amplified by PCR from mouse brain cDNA using the following primers: 5′-GTGCTTCCTCCTTGTGCTTC-3′ and 5′-CCACACTGAACAAACCAATCTG-3′. The PCR product was cloned into the pCR-BluntII-TOPO vector (Invitrogen), and the entire coding region of mouse TDP-43 was inserted in-frame into either the KpnI and XbaI sites of the pcDNA3.1/V5His vector (Invitrogen) or the KpnI and BamHI sites of the pDsRed-Monomer-Hyg-N1 vector (Clontech). An siRNA-resistant form of the TDP-43 gene was generated by changing the targeted sequence of the siRNA to 5′-GAATGACGAGCCAATTGAA-3′ (mutated nucleotides are underlined) using the KOD-Plus-Mutagenesis kit (Toyobo, Osaka, Japan).

Cell Culture and Transfection—Neuro-2a cells (American Type Culture Collection, Manassas, VA), a line derived from mouse neuroblastoma, were maintained as described previously (25). The transfection of siRNA into Neuro-2a cells was performed using Lipofectamine RNAiMAX (Invitrogen) according to the manufacturer's instructions. For the transfection of the intended plasmid and siRNA, cells were co-transfected using Lipofectamine 2000 (Invitrogen) according to the manufacturer's instructions. To differentiate the Neuro-2a cells, the medium was changed to Dulbecco's modified Eagle's medium containing 2% fetal calf serum and 20 μM retinoic acid, and cells were cultured for 24 h. For the interventional studies, the cells were incubated for 24 h with differentiation medium containing *Clostridium difficile* toxin B (Sigma-Aldrich) or for 12 h with medium containing GGTI-298 (Calbiochem). Geranylgeranyl pyrophosphate (GGPP) (Sigma-Aldrich) was added to the differentiation medium at the indicated concentration 24 h after siRNA transfection, and cells were incubated for an additional 24 h.

Quantitative Assessment of Neurite Outgrowth—Neuro-2a cells cultured in 6-well dishes were photographed using an Olympus IX71 inverted phase-contrast microscope (Olympus, Tokyo, Japan). The length of the longest neurite was measured with Image Gauge version 4.22 software (Fujifilm, Tokyo, Japan). Averages of the lengths of over 100 transfected cells were analyzed. To confirm the efficacy of siRNA transfection, BLOCK-iT™ Alexa Fluor® Red Fluorescent Control (Invitrogen) was co-transfected with TDP-43 siRNA or control RNA. The efficacy of plasmid transfection was ensured using DsRed (Clontech). To assess neurite outgrowth in TDP-43 knockdown cells, we performed a time course analysis starting at 24 h after the siRNA transfection when the differentiation medium was changed.

Cell Viability and Apoptosis Analysis—The 3-(4,5-dimethylthiazol-2-yl)-5-(3-caboxymethoxyphenyl)-2-(4-sulfophenyl)-2*H*-tetrazolium (MTS)-based cell proliferation assay was carried out on the differentiated Neuro-2a cells 48 h post-transfection using the CellTiter 96 Aqueous One Solution Cell Proliferation Assay (Promega, Madison, WI) according to the manufacturer's instructions. Absorbance at 490 nm was measured in a multiple plate reader (PowerscanHT, Dainippon Pharmaceutical). The assays were carried out in 6 wells for each condition. To assess cell apoptosis, differentiated Neuro-2a cells were stained with Alexa Fluor 488-conjugated Annexin V and with propidium iodide (PI) using the Vybrant Apoptosis Assay kit (Invitrogen) according to the manufacturer's instructions. TUNEL assays were performed using the APO-DIRECT™ kit (BD Biosciences). The extent of staining in 10,000 cells was monitored by FACSCalibur™ and CellQuest version 3.1.3 acquisition and analysis software (BD Biosciences) immediately after the staining.

Caspase-3/7 Assay—Neuro-2a cells were grown on black 96-well plates. The caspase-3/7 activity of differentiated Neuro-2a cells was analyzed using the Apo-ONE homogeneous caspase-3/7 assay (Promega) after 48 h of transfection or intended treatment according to the manufacturer's instructions. Fluorescence (485/528 nm) was measured in the multiple plate reader, and the assay was carried out in 6 wells for each condition.

Quantitative Real Time PCR—mRNA levels were determined by real time PCR as described before (26). Briefly total RNA from Neuro-2a cells was reverse transcribed into first strand cDNA, real time PCR was performed, and the product was detected by the iCycler system (Bio-Rad). For an internal standard control, the expression level of glyceraldehyde-3-phosphate dehydrogenase (GAPDH) was simultaneously quantified. The following primers were used: 5′-CCGCATGTCAGCCAAATACAAG-3′ and 5′-ACCAGAATTGGCTCCAACAACAG-3′ for TDP-43 and 5′-TGTGTCCGTCGTGGATCTGA-3′ and 5′-TTGCTGTTGAAGTCGCAGGAG-3′ for GAPDH.

Western Blot Analysis—Western blot analyses were performed as described before (27). Briefly Neuro-2a cells were lysed in Cellytic lysis buffer (Sigma-Aldrich) containing a protease inhibitor mixture (Roche Applied Science) 48 h after transfection. For subcellular fractionation, we used the Proteo-Extract Subcellular Proteome Extraction kit (Calbiochem) according to the manufacturer's instructions. Cell lysates were separated by SDS-PAGE (5–20% gradient gel) and analyzed by Western blotting with ECL Plus detection reagents (GE Healthcare). Primary antibodies used were as follows: anti-TDP-43 rabbit polyclonal antibody (1:1000; ProteinTech, Chicago, IL), anti-Rac1 mouse monoclonal antibody (1:1000; Millipore, Temecula, CA), anti-RhoA mouse monoclonal antibody (1:1000; Cytoskeleton, Denver, CO), anti-Cdc42 rabbit polyclonal antibody (1:1000; Santa Cruz Biotechnology, Santa Cruz, CA), anti-phospho-myosin phosphatase targeting subunit 1 (Thr-853) rabbit polyclonal antibody (1:500; Millipore), anti-myosin phosphatase targeting subunit 1 rabbit polyclonal antibody (1:1000; Santa Cruz Biotechnology), anti-H-Ras rabbit polyclonal antibody (1:1000; Santa Cruz Biotechnology), anti-Rab5 rabbit polyclonal antibody (1:1000; Santa Cruz Biotechnology), anti-GAPDH mouse monoclonal antibody (1:1000; BD Pharmingen) as a cytosol marker, anti-integrin β1 rabbit polyclonal antibody (1:1000; Santa Cruz Biotechnology) as a membrane marker, anti-green fluorescent protein mouse monoclonal antibody (1:2000; Millipore), anti-Rho GDP dissociation inhibitor rabbit polyclonal antibody (1:1000; Millipore), anti-geranylgeranyltransferase-1β mouse polyclonal antibody (1:1000; Abnova, Taipei, Taiwan), and anti-geranylgeranyl pyrophosphate synthase rabbit polyclonal antibody (1:1000; Abgent, San Diego, CA).

Rho Family GTPase Activation Analysis—To measure RhoA and Rac1/Cdc42 GTPase activities, we used the Rho binding domain (RBD) of the Rho effector protein with Rhotekin and Cdc42/Rac interactive binding (CRIB) region of the Cdc42/Rac effector protein with p21 activated kinase 1 (PAK), respectively. Pulldown assays were performed in the presence of glutathione *S*-transferase-tagged Rhotekin-RBD and PAK-CRIB protein-agarose beads (Cytoskeleton) according to the manufacturer's instructions.

Fluorescent Images of Neuro-2a Cells—Neuro-2a cells, which were transfected with EGFP-Rac1, DsRed-TDP-43, and siRNA (TDP-43 siRNA or control RNA), were fixed by 4% paraformaldehyde with 0.1% Triton X-100 for extraction of cytosol components. After washing, samples were mounted with VECTASHIELD mounting medium (Vector Laboratories, Inc., Burlingame, CA) and then photographed with a Zeiss Axio Imager M1 (Carl Zeiss AG).

Assay of Protein Geranylgeranylation—Neuro-2a cells were transfected with siRNA on 10-cm^2 dishes. Twenty-four hours after the transfection, 20 μM lovastatin (Sigma) was added to the culture medium. Twenty-four hours after the addition of lovastatin, the cells were labeled by adding fresh culture medium containing 6.25 μCi/ml [^{14}C]mevalonolactone (50–62 mCi/mmol) (GE Healthcare) and 20 μM lovastatin. Nineteen hours after labeling, the cells were harvested, and Rac1 was immunoprecipitated by incubating with 4 mg of anti-RhoA mouse monoclonal antibody (Santa Cruz Biotechnology) or anti-Rac1 mouse monoclonal antibody (Millipore) for 24 h followed by adding 20 μl of protein G-Sepharose (GE Healthcare). Immunoprecipitated proteins were separated by electrophoresis on a polyacrylamide-SDS gel. The ^{14}C-labeled gels were fixed and soaked in Amplify Fluorographic Reagent (GE Healthcare) for 30 min. The gels were dried, and labeled proteins were visualized on a Typhoon 9410 Workstation (GE Healthcare) after exposure to a Storage Phosphor Screen (GE Healthcare) for 72 h. We validated this experiment using 20 μM GGTI-298.

Statistical Analysis—Statistical differences (not including neurite length data) were analyzed by analysis of variance and Bonferroni post hoc analyses for three or more group comparisons and the unpaired Student's *t* test for two-group comparisons. Neurite length differences were analyzed using the Mann-Whitney *U* test (SPSS version 15.0, SPSS Inc., Chicago, IL). Two-tailed $p < 0.05$ was regarded as statistically significant.

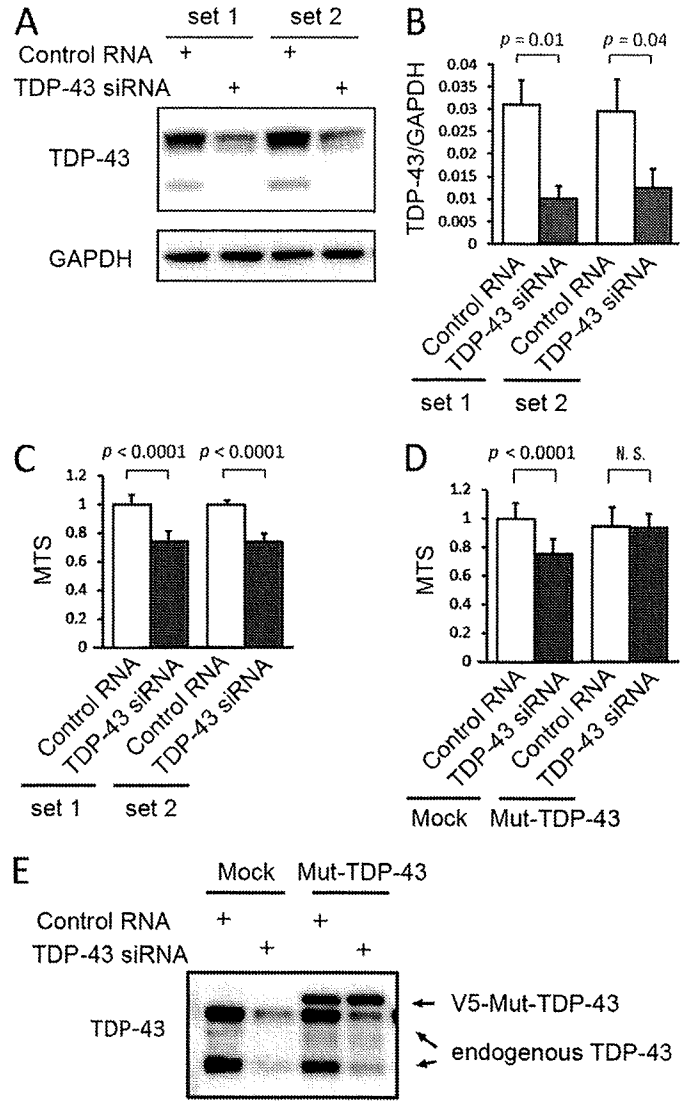

FIGURE 1. **Effects of endogenous TDP-43 depletion on cell viability.** *A*, anti-TDP-43 Western blot of Neuro-2a cells transfected with siRNAs. *B*, the mRNA expression levels of TDP-43 measured by real time RT-PCR. Data are shown as the ratio of the mRNA level of TDP-43 to that of GAPDH. *C*, the viability of Neuro-2a cells quantified by the MTS-based cell proliferation assays. TDP-43 depletion significantly reduced cell viability. *D*, a rescue experiment using the MTS assay. Mock plasmid and an siRNA-resistant form of TDP-43 (*Mut-TDP-43*) were co-transfected into Neuro-2a cells together with TDP-43 siRNA or control RNA. Mut-TDP-43 prevented the reduction of cell viability. *E*, Western blot of the cells transfected with mock plasmid or Mut-TDP-43. *Error bars* indicate S.D. *N.S.*, not significant.

RESULTS

TDP-43 Depletion Induces Cell Death and Inhibits Neurite Outgrowth—To analyze the effect of TDP-43 depletion, two sets of siRNA oligonucleotides were transfected into Neuro-2a cells. The efficiency of TDP-43 siRNA transfection was confirmed by Western blotting and quantitative real time RT-PCR (Fig. 1, *A* and *B*). To assess cell viability, we carried out an MTS-based cell proliferation assay in differentiated Neuro-2a cells after 48 h of siRNA transfection. The viability of knockdown cells was significantly decreased by both sets of siRNA compared with each control (Fig. 1*C*). To exclude the possibility of an off-target effect, a plasmid carrying an siRNA-resistant form of TDP-43 was co-transfected together with set 1 siRNA. As a result, the siRNA-resistant form of TDP-43 prevented the reduction of cell viability (Fig. 1*D*). The apoptotic process was quantified with Annexin V/PI staining and TUNEL labeling. The knockdown of TDP-43 significantly increased the number of PI-positive cells (Fig. 2*A*). However, the number of cells positive for Annexin V or TUNEL was not altered (Fig. 2, *B* and *C*). In the caspase-3/7 assay, there was no significant difference between knockdown and control cells (Fig. 2*D*). To clarify the effects of TDP-43 depletion on cellular morphology, we performed a time course experiment measuring the average length of neurites. Neurites of control cells extended over the course of 48 h, but neurite outgrowth was significantly inhibited in TDP-43-depleted cells (Fig. 2*E*).

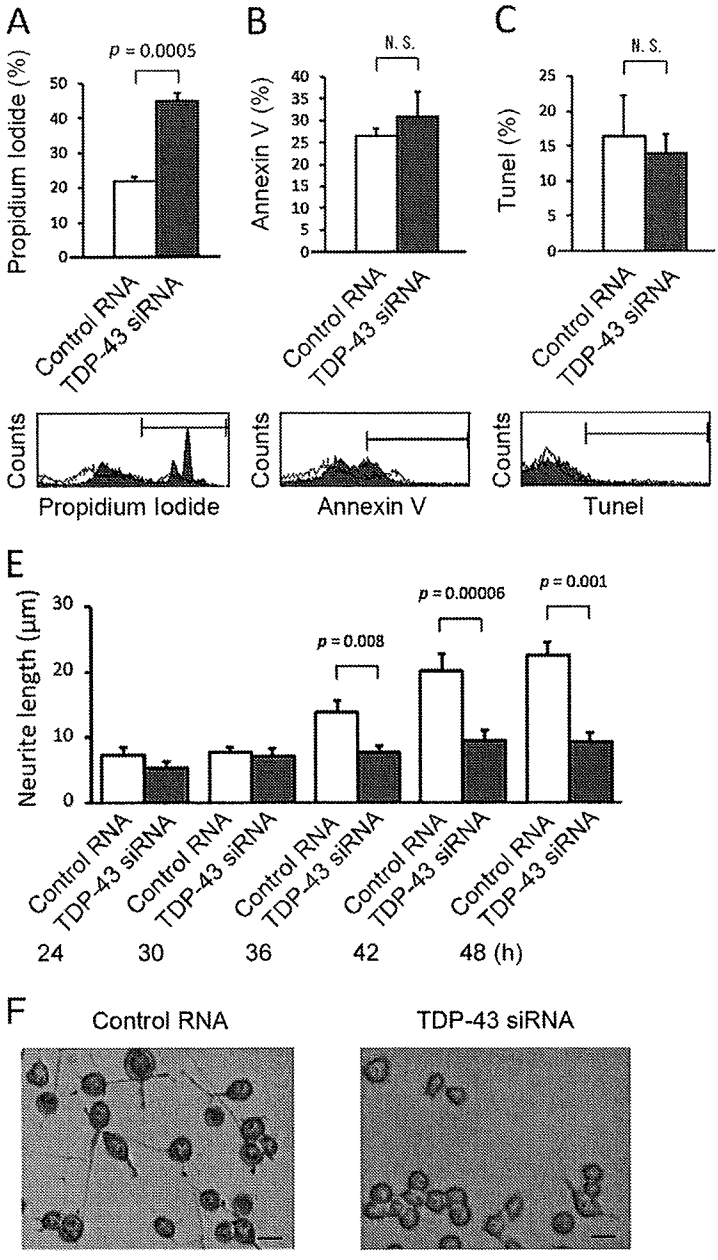

FIGURE 2. **Apoptosis analyses and quantitative assessment of neurite outgrowth in TDP-43-depleted Neuro-2a cells.** *A*, *B*, and *C*, the number of the cells positive for PI, Annexin V, and TUNEL staining. We counted 10,000 cells using flow cytometry. Knockdown of TDP-43 significantly increased the number of cells stained with PI but not that with stained with Annexin V or TUNEL. *D*, caspase-3/7 activity of Neuro-2a cells transfected with TDP-43 siRNA or control RNA. *E*, time course analysis of neurite outgrowth in Neuro-2a cells transfected with TDP-43 siRNA or control RNA. Averages of the longest neurite lengths of over 100 transfected cells were analyzed 24 h after the transfection of siRNA. Neurites of control cells extended over the course of 48 h, but in TDP-43-depleted cells, neurite outgrowth was inhibited. *Error bars* indicate S.D. (*A–D*) or S.E. (*E*). *F*, phase-contrast images of Neuro-2a cells 48 h after the transfection of control RNA or TDP-43 siRNA. *Scale bar*, 10 μm. *N.S.*, not significant.

Knockdown of TDP-43 Reduces Rho Family GTPase Activity—To elucidate the pathophysiology of neuronal cell death and the morphological alteration caused by TDP-43 depletion, we focused on the Rho family GTPases, which are potent regulators of neurite outgrowth and cell survival. First RhoA, Rac1, and Cdc42 GTPase activities were investigated by pulldown assays. In TDP-43-depleted cells, the activities of RhoA, Rac1, and Cdc42 GTPase were all decreased compared with the controls (Fig. 3, *A* and *B*). Inactivation of RhoA GTPase was also confirmed by a significant reduction in the level of the Thr-853 phosphorylation of myosin phosphatase targeting subunit 1, which is exclusively phosphorylated by Rho kinase (28) (Fig. 3*A*). To verify that inactivation of Rho family GTPases leads to neuronal damage, we tested the effects of *C. difficile* toxin B, a pan-inhibitor of Rho family proteins, on differentiated Neuro-2a cells. As a result, this toxin reduced cell viability and inhibited neurite outgrowth (Fig. 3, *C* and *D*).

Small G proteins, including Rho and Ras family members, must be able to localize at the cell membrane to exert their biological functions (29). We thus investigated the intracellular distribution of Rho family proteins to elucidate the mechanism by which TDP-43 regulates their GTPase activity. Western blots showed that the amounts of RhoA, Rac1, and Cdc42, but not H-Ras or Rab5, in the membrane fractions were decreased in the TDP-43 knockdown cells (Fig. 4*A*). The subcellular fraction of Rho GDP dissociation inhibitor, another regulator of Rho activity, was not altered by TDP-43 knockdown (Fig. 4*A*). The siRNA-resistant form of TDP-43 rescued the reduction in the amount of membrane-bound Rho family GTPases (Fig. 4*B*). The fluorescent images also demonstrated that membrane-localized Rac1 was significantly reduced in TDP-43 knockdown cells in comparison with control cells (Fig. 5).

TDP-43 Regulates Rho GTPase Activity via Protein Geranylgeranylation—For membrane localization to occur, members of the Rho family of GTPases have to be catalyzed by transferring GGPP to the C-terminal motif (geranylgeranylation), whereas Ras family members, such as H-Ras, require farnesyl pyrophosphate. We thus tested two agents that modulate geranylgeranylation of Rho family molecules. GGTI-298, a specific inhibitor of geranylgeranylation, has been shown to increase neural cell death through the inactivation of Rho family GTPases (30, 31). In differentiated Neuro-2a cells, GGTI-298 inhibited neurite outgrowth and reduced cell viability in a dose-dependent manner without any evidence of caspase-3/7 activation (Fig. 6, *A–C*). GGTI-298 also decreased the amount of membrane-

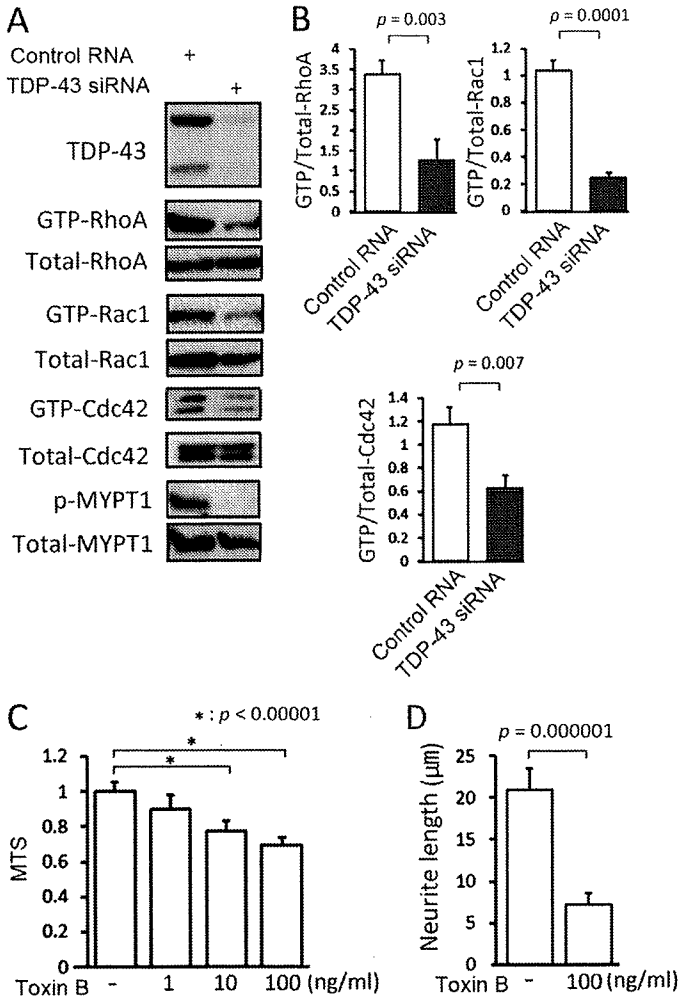

FIGURE 3. **Activities of Rho family GTPases in TDP-43-depleted Neuro-2a cells.** *A*, pulldown assays of RhoA, Rac1, and Cdc42 and Western blot using anti-phospho-myosin phosphatase targeting subunit 1 (*p-MYPT1*) in Neuro-2a cells transfected with TDP-43 siRNA or control RNA. TDP-43 knockdown significantly reduced Rho family GTPase activity. *B*, densitometric quantitations of three independent experiments. *C*, the viabilities of Neuro-2a cells incubated with the indicated concentrations of *C. difficile* toxin B. *D*, quantitation of neurite outgrowth in Neuro-2a cells incubated with 100 ng/ml toxin B compared with control. *Error bars* indicate S.D. (*B* and *C*) or S.E. (*D*).

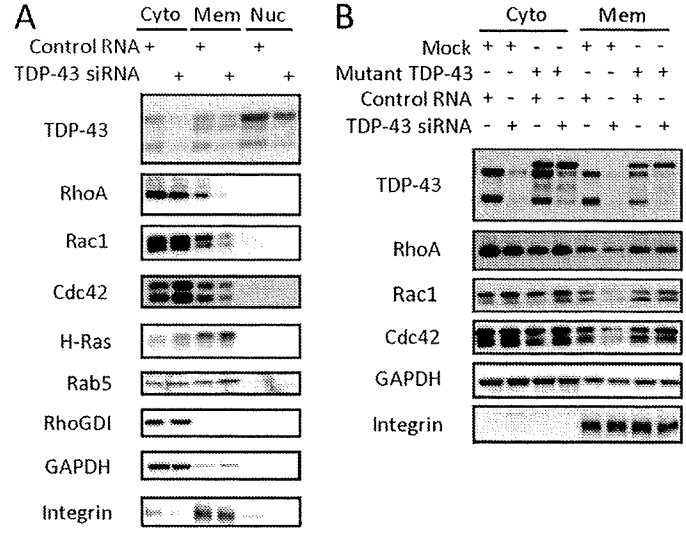

FIGURE 4. **Intracellular distribution of Rho family GTPases in TDP-43 knockdown Neuro-2a cells.** *A*, Western blots of subcellular fractions (cytosol, membrane, and nucleus) of Neuro-2a cells transfected with TDP-43 siRNA or control RNA. The amount of Rho family members in the membrane fraction was significantly reduced in TDP-43 knockdown cells. This effect, however, was not observed with H-Ras or Rab5. Moreover the subcellular fraction of Rho GDP dissociation inhibitor (*RhoGDI*) was not altered by TDP-43 depletion. GAPDH and integrin β1 were used as a cytosol and membrane marker, respectively. *Cyto*, cytosol fraction; *Mem*, membrane fraction; *Nuc*, nuclear fraction. *B*, the effect of the siRNA-resistant form of TDP-43 (*Mut-TDP-43*) on the intracellular distribution of Rho family GTPases. Mut-TDP-43 prevented the reduction of membrane-bound Rho family members.

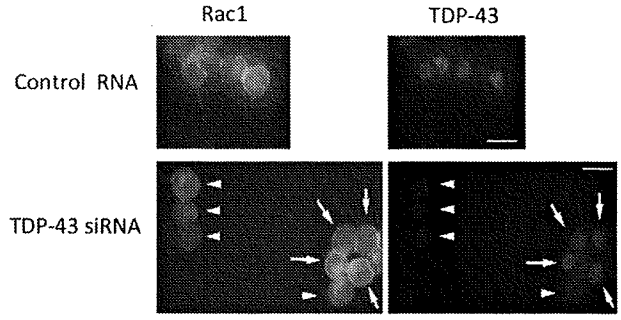

FIGURE 5. **Fluorescent images of Neuro-2a cells.** Neuro-2a cells co-transfected with EGFP-Rac1, DsRed-TDP-43, and siRNA (TDP-43 siRNA or control RNA) were fixed by 4% paraformaldehyde with 0.1% Triton X-100. Membrane-localized Rac1 was significantly reduced in the TDP-43 depleted cells (*arrowhead*) compared with the cells that escaped knockdown of TDP-43 (*arrow*) and with the control RNA-transfected cells. *Scale bar*, 10 μm.

bound Rho GTPases (Fig. 6*D*). In contrast, GGPP, the final substrate of geranylgeranylation, prevented the reduction in the amounts of membrane-bound RhoA, Rac1, and Cdc42 caused by TDP-43 knockdown (Fig. 6*E*). In addition, GGPP restored viability and neurite outgrowth in TDP-43-depleted cells (Fig. 6, *F* and *G*). These findings indicate that impaired geranylgeranylation appears to be the molecular basis of TDP-43 depletion-induced cellular damage. We next examined whether TDP-43 regulates geranylgeranylation of Rho GTPases. Fig. 7, *A–C*, shows that TDP-43 increased the amount of membrane-bound Rho GTPases, augmented neurite outgrowth, and increased cell viability in GGTI-298-treated cells.

Taken together, these observations suggest that TDP-43 regulates the activities of Rho family members through protein geranylgeranylation. We thus investigated the effect of TDP-43 depletion on protein geranylgeranylation using [^{14}C]mevalonic acid (MVA). Incorporation of [^{14}C]MVA into RhoA or Rac1 was significantly decreased in the TDP-43-depleted Neuro-2a cells (Fig. 8, *A* and *B*), suggesting that the knockdown of TDP-43 inhibits geranylgeranylation of Rho family members. GGTI-298 reduced incorporation of [^{14}C]MVA into Rac1, further confirming this conclusion (Fig. 8*C*).

Protein geranylgeranylation of the Rho family is regulated by specific enzymes: geranylgeranyltransferase-Iβ and geranylgeranyl pyrophosphate synthase-1, which is responsible for synthesis of GGPP. We therefore investigated the expression levels of these enzymes. However, the knockdown of TDP-43 did not alter the protein expression level of geranylgeranyltransferase-Iβ or geranylgeranyl pyrophosphate synthase-1 (data not shown).

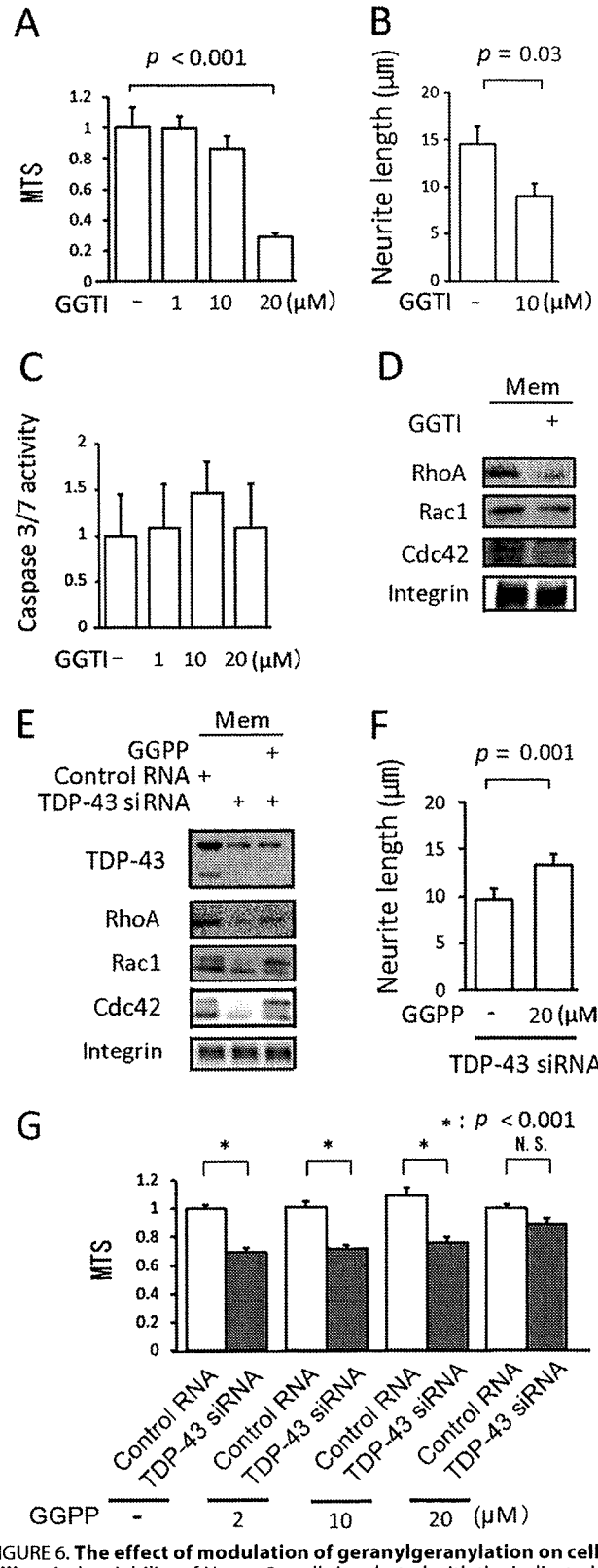

FIGURE 6. **The effect of modulation of geranylgeranylation on cell viability.** *A*, the viability of Neuro-2a cells incubated with the indicated concentrations of GGTI-298 (*GGTI*). *B*, averages of neurite length in Neuro-2a cells incubated with 20 μM GGTI-298 compared with control. *C*, caspase-3/7 activity in Neuro-2a cells treated with GGTI-298. *D*, Western blot of the membrane fraction from Neuro-2a cells incubated with 20 μM GGTI-298 compared with control. *E*, Western blot of the membrane fraction from Neuro-2a cells incubated with 20 μM GGPP in the presence of TDP-43 siRNA. *F*, measurement of neurite length of Neuro-2a cells incubated with 20 μM GGPP. The cells were transfected with TDP-43 siRNA or control RNA. *G*, the viability of Neuro-2a cells incubated with the indicated concentrations of GGPP. *Error bars* indicate S.D. (*A* and *C*) or S.E. (*B* and *F*). *N.S.*, not significant.

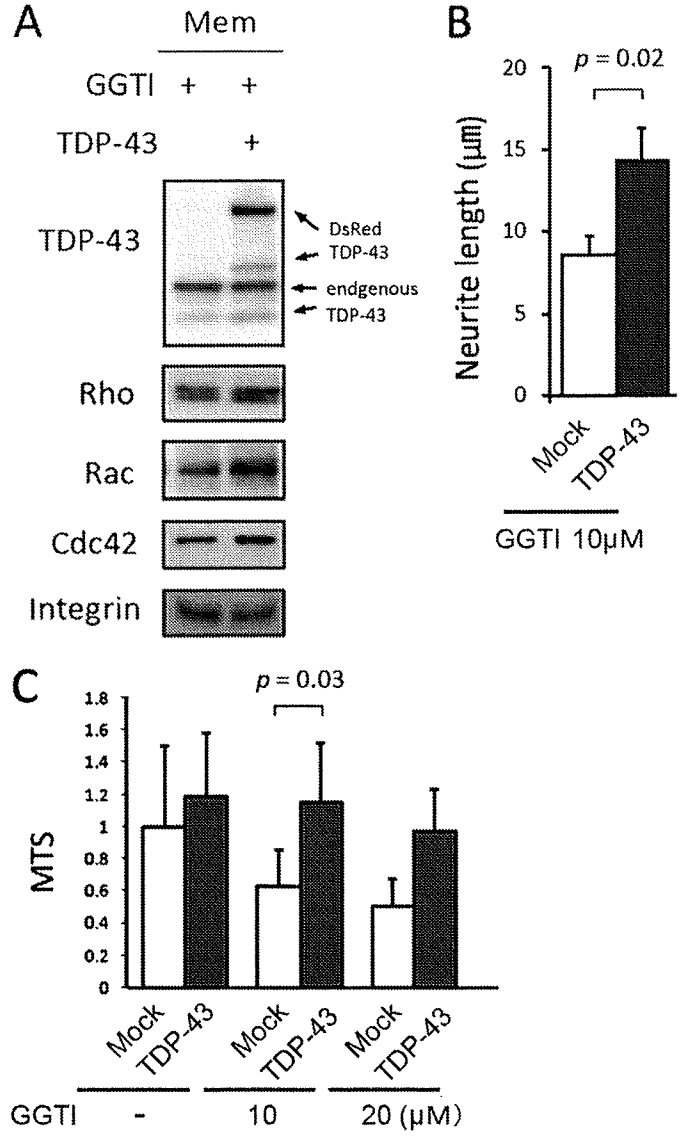

FIGURE 7. **Effect of TDP-43 in Neuro-2a cells on GGTI-298-induced cellular phenotype.** *A*, Western blot of the membrane (*Mem*) fraction of 10 μM GGTI-298 (*GGTI*)-treated Neuro-2a cells transfected with TDP-43 or mock vector. *B*, neurite length of GGTI-298-treated Neuro-2a cells transfected with DsRed-TDP-43 or mock vector. *C*, the viability of Neuro-2a cells incubated with the indicated concentrations of GGTI-298. *Error bars* indicate S.E. (*B*) or S.D. (*C*).

DISCUSSION

TDP-43 as a Regulator of Rho Family GTPases—In the present study, we demonstrated that knockdown of TDP-43 inhibits neurite outgrowth and induces cell death in differentiated Neuro-2a cells, suggesting that loss of TDP-43 function plays a causative role in neurodegeneration. To elucidate the molecular mechanisms by which TDP-43 depletion causes neuronal cell damage, we examined the relationship between TDP-43 and Rho family GTPases. Neuronal morphology is determined in large part through the regulation of the cytoskeleton. One of the key regulators of the actin cytoskeleton is the Rho family of GTPases: RhoA, Rac1, and Cdc42 (15–17). Although each Rho

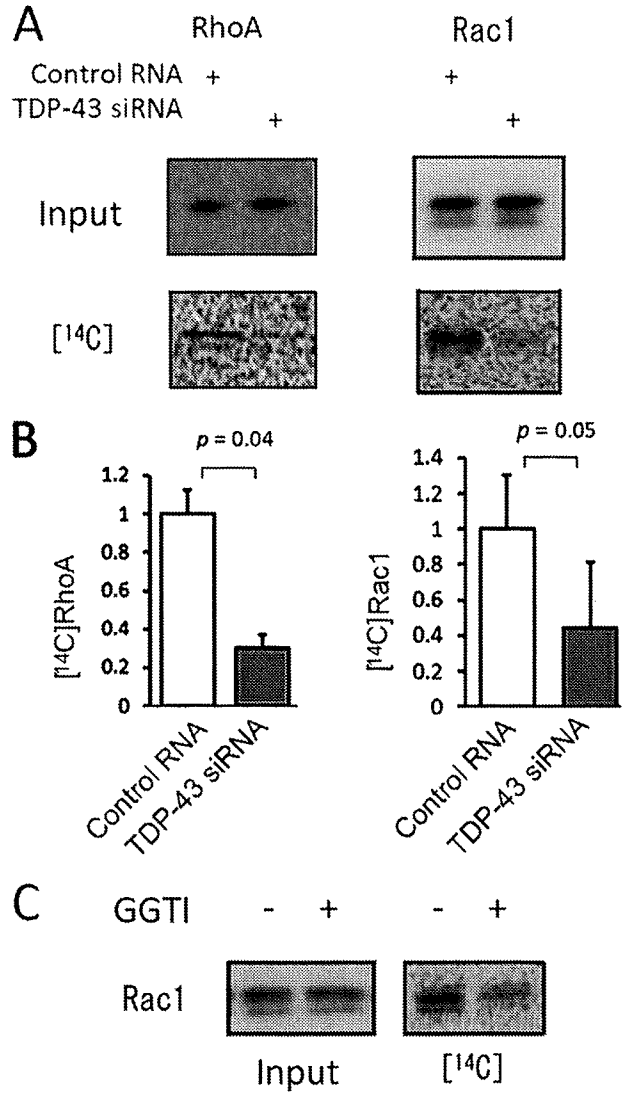

FIGURE 8. **Protein prenylation of RhoA and Rac1 in Neuro-2a cells.** *A*, Neuro-2a cells were metabolically labeled with [^{14}C]MVA: *left*, Western blot with anti-RhoA or Rac1 antibody of cell lysates; *right*, incorporation of [^{14}C]MVA into RhoA or Rac1. *B*, densitometric quantitation of four independent experiments. *Error bars* indicate S.D. *C*, incorporation of [^{14}C]MVA into Rac1 in Neuro-2a cells incubated with or without GGTI-298 (*GGTI*).

family member has a distinct effect on cell morphology and plays an important role in the regulation of neuronal survival, we demonstrated that pan-inhibition of Rho family proteins by *C. difficile* toxin B suppressed neurite outgrowth and reduced cell viability as reported previously (19–21, 32, 33). We demonstrated here that the activities of RhoA, Rac1, and Cdc42 were all decreased in TDP-43-depleted cells, suggesting that knockdown of TDP-43 induces inhibition of neurite outgrowth and cell death through the inactivation of Rho family GTPases. There was no evidence of apoptosis mediated by TDP-43 knockdown in the model we used perhaps because of the biological characteristics of Neuro-2a cells in which the induction of apoptosis is known to be difficult (34, 35). In support of this view, we confirmed that GGTI-298 had no effect on apoptosis in Neuro-2a cells under the present conditions (Fig. 6*C*), although this reagent has been shown to efficiently induce apoptosis in non-neuronal cells (36, 37).

Inhibited Protein Geranylgeranylation of Rho Family Members in TDP-43-depleted Cells—How does TDP-43 regulate the activities of the Rho family? Various molecules have been shown to regulate the activity of Rho, Rac, and Cdc42, but few are capable of regulating all three GTPases concomitantly. To elucidate the molecular mechanism by which TDP-43 regulates Rho, Rac, and Cdc42, we directed our attention to the fact that membrane localization is the key regulatory factor common to these molecules. Small G proteins, including members of the Rho and Ras families, act as molecular switches cycling between an active, GTP-bound state and an inactive, GDP-bound state (18, 38, 39). Post-translational modification with a C-terminal prenyl moiety allows small G proteins to associate with the membrane where they can interact with and activate their effectors (29). Proteins that require prenylation include the farnesyl group, such as the Ras family, and the geranylgeranyl group, such as the Rho or the Rab family (29, 40). In the present study, we showed that knockdown of TDP-43 decreased membrane-bound RhoA, Rac1, and Cdc42 but did not affect the intracellular distribution of H-Ras or Rab5. TDP-43 knockdown also inhibited the incorporation of [^{14}C]MVA, a tracer of the mevalonate pathway, into RhoA and Rac1 in differentiated Neuro-2a cells. In contrast, the expression level of Rho GDP dissociation inhibitor, which functions by extracting Rho family GTPases from membranes and solubilizing them in the cytosol (41, 42), was not significantly altered by TDP-43 knockdown. In addition, inhibition of geranylgeranylation by GGTI-298 reproduced the cytotoxic effects of TDP-43 depletion, whereas GGPP, the substrate of the geranylgeranylation pathway, restored cell viability and neurite outgrowth in TDP-43-depleted Neuro-2a cells. Furthermore in GGTI-298 treated cells, overexpression of TDP-43 restored the membrane localization of Rho GTPases as well as cell viability and neurite outgrowth. These findings suggest that TDP-43 depletion inactivates Rho family GTPases through inhibition of protein geranylgeranylation.

Protein geranylgeranylation of Rho family members is catalyzed by geranylgeranyltransferase-I using GGPP produced by geranylgeranyl pyrophosphate synthase-1 as the substrate (43). Geranylgeranyltransferase-I consists of two subunits, α and β, and the α subunit is also a component of protein farnesyltransferase (44). We thus assessed the mRNA and protein expression of geranylgeranyltransferase-Iβ and geranylgeranyl pyrophosphate synthase-1 in Neuro-2a cells. However, the expression levels of these enzymes were not altered by TDP-43 knockdown. These results imply that TDP-43 depletion decreases the activities of these enzymes.

Loss of TDP-43 Function in the Pathophysiology of TDP-43 Proteinopathies—Ubiquitinated cytoplasmic inclusions are a histopathological hallmark of ALS and frontotemporal lobar degeneration with ubiquitin-positive inclusions. Although the nature of these aggregates has not been fully elucidated, recent studies have identified TDP-43 as the major component of the ubiquitin-immunoreactive neuronal inclusions seen in ALS and frontotemporal lobar degeneration with ubiquitin-positive inclusions (1, 2). There has been a great deal of debate about whether loss or gain of function of TDP-43 causes neuronal dysfunction and eventual cell death. Although TDP-43 is a

ubiquitously expressed, highly conserved nuclear protein, under the pathological conditions in ALS and frontotemporal lobar degeneration with ubiquitin-positive inclusions, TDP-43 completely disappears from the nuclei of the affected neurons (1, 2). These histopathological findings indicate that loss of nuclear TDP-43 may underlie neuronal degeneration, although it is also possible that neuronal inclusions possess cytotoxic properties. It has been reported that TDP-43 depletion leads to up-regulation of cyclin-dependent kinase 6 protein and transcript levels followed by misregulation of the cell cycle and apoptosis in cultured human epithelial cancer cells (14). In the present study, knockdown of TDP-43 inactivated Rho family GTPases and thereby induced cell death in differentiated Neuro-2a cells. Although this is not the model imitating the dislocation of TDP-43 from the nucleus to the cytoplasm, our findings suggest that loss of function of TDP-43 may induce neuronal degeneration probably through dysregulation of Rho family GTPases.

In summary, we have demonstrated that TDP-43 depletion inhibits neurite outgrowth and induces neuronal cell death. This phenomenon possibly results from a reduced membrane localization of Rho family GTPases due to the inhibition of protein geranylgeranylation.

REFERENCES

1. Neumann, M., Sampathu, D. M., Kwong, L. K., Truax, A. C., Micsenyi, M. C., Chou, T. T., Bruce, J., Schuck, T., Grossman, M., Clark, C. M., McCluskey, L. F., Miller, B. L., Masliah, E., Mackenzie, I. R., Feldman, H., Feiden, W., Kretzschmar, H. A., Trojanowski, J. Q., and Lee, V. M. (2006) *Science* **314,** 130–133
2. Arai, T., Hasegawa, M., Akiyama, H., Ikeda, K., Nonaka, T., Mori, H., Mann, D., Tsuchiya, K., Yoshida, M., Hashizume, Y., and Oda, T. (2006) *Biochem. Biophys. Res. Commun.* **351,** 602–611
3. Gitcho, M. A., Baloh, R. H., Chakraverty, S., Mayo, K., Norton, J. B., Levitch, D., Hatanpaa, K. J., White, C. L., 3rd, Bigio, E. H., Caselli, R., Baker, M., Al-Lozi, M. T., Morris, J. C., Pestronk, A., Rademakers, R., Goate, A. M., and Cairns, N. J. (2008) *Ann. Neurol.* **63,** 535–538
4. Yokoseki, A., Shiga, A., Tan, C. F., Tagawa, A., Kaneko, H., Koyama, A., Eguchi, H., Tsujino, A., Ikeuchi, T., Kakita, A., Okamoto, K., Nishizawa, M., Takahashi, H., and Onodera, O. (2008) *Ann. Neurol.* **63,** 538–542
5. Kabashi, E., Valdmanis, P. N., Dion, P., Spiegelman, D., McConkey, B. J., Vande Velde, C., Bouchard, J. P., Lacomblez, L., Pochigaeva, K., Salachas, F., Pradat, P. F., Camu, W., Meininger, V., Dupre, N., and Rouleau, G. A. (2008) *Nat. Genet.* **40,** 572–574
6. Sreedharan, J., Blair, I. P., Tripathi, V. B., Hu, X., Vance, C., Rogelj, B., Ackerley, S., Durnall, J. C., Williams, K. L., Buratti, E., Baralle, F., de Belleroche, J., Mitchell, J. D., Leigh, P. N., Al-Chalabi, A., Miller, C. C., Nicholson, G., and Shaw, C. E. (2008) *Science* **319,** 1668–1672
7. Van Deerlin, V. M., Leverenz, J. B., Bekris, L. M., Bird, T. D., Yuan, W., Elman, L. B., Clay, D., Wood, E. M., Chen-Plotkin, A. S., Martinez-Lage, M., Steinbart, E., McCluskey, L., Grossman, M., Neumann, M., Wu, I. L., Yang, W. S., Kalb, R., Galasko, D. R., Montine, T. J., Trojanowski, J. Q., Lee, V. M., Schellenberg, G. D., and Yu, C. E. (2008) *Lancet Neurol.* **7,** 409–416
8. Ayala, Y. M., Pantano, S., D'Ambrogio, A., Buratti, E., Brindisi, A., Marchetti, C., Romano, M., and Baralle, F. E. (2005) *J. Mol. Biol.* **348,** 575–588
9. Buratti, E., Brindisi, A., Giombi, M., Tisminetzky, S., Ayala, Y. M., and Baralle, F. E. (2005) *J. Biol. Chem.* **280,** 37572–37584
10. Wang, I. F., Reddy, N. M., and Shen, C. K. (2002) *Proc. Natl. Acad. Sci. U.S.A.* **99,** 13583–13588
11. Wang, H. Y., Wang, I. F., Bose, J., and Shen, C. K. (2004) *Genomics* **83,** 130–139
12. Bose, J. K., Wang, I. F., Hung, L., Tarn, W. Y., and Shen, C. K. (2008) *J. Biol. Chem.* **283,** 28852–28859
13. Strong, M. J., Volkening, K., Hammond, R., Yang, W., Strong, W., Leystra-Lantz, C., and Shoesmith, C. (2007) *Mol. Cell. Neurosci.* **35,** 320–327
14. Ayala, Y. M., Misteli, T., and Baralle, F. E. (2008) *Proc. Natl. Acad. Sci. U.S.A.* **105,** 3785–3789
15. Kaibuchi, K., Kuroda, S., and Amano, M. (1999) *Annu. Rev. Biochem.* **68,** 459–486
16. Burridge, K., and Wennerberg, K. (2004) *Cell* **116,** 167–179
17. Jaffe, A. B., and Hall, A. (2005) *Annu. Rev. Cell Dev. Biol.* **21,** 247–269
18. Hall, A. (1998) *Science* **279,** 509–514
19. Just, I., Selzer, J., Wilm, M., von Eichel-Streiber, C., Mann, M., and Aktories, K. (1995) *Nature* **375,** 500–503
20. Bradke, F., and Dotti, C. G. (1999) *Science* **283,** 1931–1934
21. Ahmed, I., Calle, Y., Iwashita, S., and Nur-E-Kamal, A. (2006) *Mol. Cell. Biochem.* **281,** 17–25
22. Cairns, N. J., Neumann, M., Bigio, E. H., Holm, I. E., Troost, D., Hatanpaa, K. J., Foong, C., White, C. L., 3rd, Schneider, J. A., Kretzschmar, H. A., Carter, D., Taylor-Reinwald, L., Paulsmeyer, K., Strider, J., Gitcho, M., Goate, A. M., Morris, J. C., Mishra, M., Kwong, L. K., Stieber, A., Xu, Y., Forman, M. S., Trojanowski, J. Q., Lee, V. M., and Mackenzie, I. R. (2007) *Am. J. Pathol.* **171,** 227–240
23. Nakagawa, M., Fukata, M., Yamaga, M., Itoh, N., and Kaibuchi, K. (2001) *J. Cell Sci.* **114,** 1829–1838
24. Watanabe, T., Wang, S., Noritake, J., Sato, K., Fukata, M., Takefuji, M., Nakagawa, M., Izumi, N., Akiyama, T., and Kaibuchi, K. (2004) *Dev. Cell* **7,** 871–883
25. Niwa, J., Yamada, S., Ishigaki, S., Sone, J., Takahashi, M., Katsuno, M., Tanaka, F., Doyu, M., and Sobue, G. (2007) *J. Biol. Chem.* **282,** 28087–28095
26. Katsuno, M., Adachi, H., Minamiyama, M., Waza, M., Tokui, K., Banno, H., Suzuki, K., Onoda, Y., Tanaka, F., Doyu, M., and Sobue, G. (2006) *J. Neurosci.* **26,** 12106–12117
27. Katsuno, M., Adachi, H., Doyu, M., Minamiyama, M., Sang, C., Kobayashi, Y., Inukai, A., and Sobue, G. (2003) *Nat. Med.* **9,** 768–773
28. Feng, J., Ito, M., Ichikawa, K., Isaka, N., Nishikawa, M., Hartshorne, D. J., and Nakano, T. (1999) *J. Biol. Chem.* **274,** 37385–37390
29. Adamson, P., Marshall, C. J., Hall, A., and Tilbrook, P. A. (1992) *J. Biol. Chem.* **267,** 20033–20038
30. Tanaka, T., Tatsuno, I., Uchida, D., Moroo, I., Morio, H., Nakamura, S., Noguchi, Y., Yasuda, T., Kitagawa, M., Saito, Y., and Hirai, A. (2000) *J. Neurosci.* **20,** 2852–2859
31. Meske, V., Albert, F., Richter, D., Schwarze, J., and Ohm, T. G. (2003) *Eur. J. Neurosci.* **17,** 93–102
32. Linseman, D. A., Laessig, T., Meintzer, M. K., McClure, M., Barth, H., Aktories, K., and Heidenreich, K. A. (2001) *J. Biol. Chem.* **276,** 39123–39131
33. Loucks, F. A., Le, S. S., Zimmermann, A. K., Ryan, K. R., Barth, H., Aktories, K., and Linseman, D. A. (2006) *J. Neurochem.* **97,** 957–967
34. Sueyoshi, N., Maehara, T., and Ito, M. (2001) *J. Lipid Res.* **42,** 1197–1202
35. Saito, M., Saito, M., Cooper, T. B., and Vadasz, C. (2005) *Alcohol Clin. Exp. Res.* **29,** 1374–1383
36. Xia, Z., Tan, M. M., Wong, W. W., Dimitroulakos, J., Minden, M. D., and Penn, L. Z. (2001) *Leukemia* **15,** 1398–1407
37. Li, X., Liu, L., Tupper, J. C., Bannerman, D. D., Winn, R. K., Sebti, S. M., Hamilton, A. D., and Harlan, J. M. (2002) *J. Biol. Chem.* **277,** 15309–15316
38. Lamarche, N., and Hall, A. (1994) *Trends Genet* **10,** 436–440
39. Zhou, K., Wang, Y., Gorski, J. L., Nomura, N., Collard, J., and Bokoch, G. M. (1998) *J. Biol. Chem.* **273,** 16782–16786
40. Cox, A. D., and Der, C. J. (1992) *Curr. Opin. Cell Biol.* **4,** 1008–1016
41. Fukumoto, Y., Kaibuchi, K., Hori, Y., Fujioka, H., Araki, S., Ueda, T., Kikuchi, A., and Takai, Y. (1990) *Oncogene* **5,** 1321–1328
42. Dovas, A., and Couchman, J. R. (2005) *Biochem. J.* **390,** 1–9
43. Ericsson, J., Greene, J. M., Carter, K. C., Shell, B. K., Duan, D. R., Florence, C., and Edwards, P. A. (1998) *J. Lipid Res.* **39,** 1731–1739
44. Moomaw, J. F., and Casey, P. J. (1992) *J. Biol. Chem.* **267,** 17438–17443

Journal of the Neurological Sciences 276 (2009) 163–169

Contents lists available at ScienceDirect

Journal of the Neurological Sciences

journal homepage: www.elsevier.com/locate/jns

Age at onset influences on wide-ranged clinical features of sporadic amyotrophic lateral sclerosis

Naoki Atsuta [a], Hirohisa Watanabe [a], Mizuki Ito [a], Fumiaki Tanaka [a], Akiko Tamakoshi [b], Imaharu Nakano [c], Masashi Aoki [d], Shoji Tsuji [e], Tatsuhiko Yuasa [f], Hiroki Takano [g], Hideaki Hayashi [h], Shigeki Kuzuhara [i], Gen Sobue [a,*]
Research Committee on the Neurodegenerative Diseases of Japan

[a] Department of Neurology, Nagoya University Graduate School of Medicine, Nagoya, Japan
[b] Department of Public Health, Aichi Medical University, Aichi, Japan
[c] Division of Neurology, Department of Medicine, Jichi Medical University School of Medicine, Tochigi, Japan
[d] Department of Neurology, Tohoku University School of Medicine, Sendai, Japan
[e] Department of Neurology, Graduate School of Medicine, University of Tokyo, Tokyo, Japan
[f] Kohnodai Hospital, National Center of Neurology and Psychiatry, Tokyo, Japan
[g] Department of Neurology, Brain Research Institute, Niigata University, Niigata, Japan
[h] Department of Neurology, Tokyo Metropolitan Neurological Hospital, Tokyo, Japan
[i] Musashi Hospital, National Center of Neurology and Psychiatry, Tokyo, Japan

ARTICLE INFO

Article history:
Received 17 March 2008
Received in revised form 19 July 2008
Accepted 16 September 2008
Available online 28 October 2008

Keywords:
ALS
Japan
Sporadic
Age at onset
Initial symptom
Clinical feature
TPPV

ABSTRACT

Purpose: To profile the detailed clinical features of sporadic amyotrophic lateral sclerosis (ALS) on large-scale samples in Japan.
Methods: We assessed the clinical features of sporadic ALS patients in Japan, based on the nationwide registration system of the Ministry of Health, Labor and Welfare of Japan. We described 3428 new cases registered cases between 2003 and 2006 to analyze initial symptoms and related clinical features, 4202 cases registered in the single year of 2005 to describe the cross-sectional overview of the ALS patients, and a total of 2128 cases with tracheostomy positive pressure ventilation (TPPV) from all of the registration data from 2003 to 2006 to describe the features of ALS patients with TPPV.
Results: The patients with an older age at onset progressed more rapidly to the TPPV stage than those with a younger age at onset. The subpopulation of patients with long-standing TPPV showed ophthalmoplegia, while its appearance rate was less in the patients with an older age at onset than in those with a younger age at onset. Furthermore, age at onset strongly influenced the frequency of initial symptoms: dysarthria, dysphagia, neck weakness and respiratory disturbance were more frequent in patients with an older age at onset, while upper or lower limb weakness was observed more frequently in patients with a younger age at onset. In addition, those initial symptoms were still the most prominent at the follow-up stage, suggesting that the initial symptoms determine the major clinical features even in advanced illness.
Conclusions: Our present study demonstrated that symptomatic features of ALS are strongly influenced by the age at onset by the large scale of samples.

1. Introduction

Amyotrophic lateral sclerosis (ALS) is one of the most devastating neurodegenerative diseases affecting upper and lower motor neurons preferentially, and shows progressive muscle wasting of the limb, bulbar and respiratory musculatures. Almost half of ALS patients expire within three years of onset, primarily due to respiratory failure [1–6]. Approximately 5–10% of ALS patients show a familial trait, while more than 90% of the patients are sporadic, and the causal mechanism of the motor neuron degeneration is largely unknown. Although many clinical trials of potential therapeutic agents for the treatment of sporadic ALS have been performed [7], effective therapeutics against motor neuron degeneration in ALS except for riluzole [8,9] have not been developed. The clinical features of ALS have been established for the most part. However, many aspects of symptomatic manifestations such as the influence of age at onset on clinical features, the frequency of rare symptoms and many other symptomatic details have not been well characterized, particularly

Abbreviations: ALS, amyotrophic lateral sclerosis; TPPV, tracheostomy positive pressure ventilation.

* Corresponding author. Department of Neurology, Nagoya University Graduate School of Medicine, Nagoya 466-8550 Japan. Fax: +81 52 744 2384.
E-mail address: sobueg@med.nagoya-u.ac.jp (G. Sobue).

0022-510X/$ – see front matter © 2008 Elsevier B.V. All rights reserved.
doi:10.1016/j.jns.2008.09.024